Informatics in Medicine Unlocked 15 (2019) 100185

Contents lists available at ScienceDirect

Informatics in Medicine Unlocked

journal homepage: www.elsevier.com/locate/imu

A finite element study of posterior eye biomechanics: The influence of intraocular and cerebrospinal pressure on the optic nerve head, peripapillary region, subarachnoid space and meninges

Diana Marcela Muñoz-Sarmiento[a,*,1], Óscar Libardo Rodríguez-Montaño[a], Juan David Alarcón-Castiblanco[a], Miguel Alejandro Gamboa-Márquez[b], Jennifer Paola Corredor-Gómez[b], Carlos Julio Cortés-Rodríguez[a]

[a] National University of Colombia, Bogotá Colombia, Department of Mechanical Engineering and Mechatronics. Biomechanics Research Group, Colombia
[b] GATAcorp. Bogota, Colombia

ARTICLE INFO

Keywords:
Glaucoma
Physiopathology
Choroid
Retina
Sclera
Meninges
Subarachnoid space

ABSTRACT

Several biomechanical factors have been associated with the development of glaucoma. However, although optic nerve head (ONH) biomechanics have been previously analysed, other ocular zones have been less explored. Therefore, in this study, the effect of intraocular and cerebrospinal fluid pressure (CSFP) on the ONH, peripapillary region (PPR), optic nerve subarachnoid space (SAS) and meninges have been investigated. Two finite element models of the eye were made from one anatomical configuration, including the complete PPR (choroid, retina, and sclera), all meningeal layers and the SAS. Each of the models were subjected to 12 different eye pressures, and one model was additionally subjected to 20 cerebrospinal pressures. Furthermore, the biomechanical impact of each meningeal layer and SAS on the ONH and PPR was assessed. Global results indicated that the greatest strains occurred in the retina, followed by the prelaminar region and lamina cribrosa (LC). With an increase in intraocular pressure (IOP), all of the PPR showed thinning; nevertheless, the retina was the layer most affected. Additionally, the results showed that the postlaminar tissue was the region most deformed by CSFP variations. Despite this, a low CSFP, associated with ocular hypertension, caused an increase in retinal, choroidal and LC strains, and posterior displacement of central and medial regions of the LC and prelaminar tissue, as well as a change in postlaminar tissue biomechanics. Finally, the meninges produced an important reduction in ONH strains due to IOP fluctuations, and variations in SAS stiffness had a strong influence on strains within the ONH and PPR.

1. Introduction

Glaucoma is currently the leading cause of irreversible blindness worldwide and so is a very active area of research [1]. It produces an increase in excavation of the optic nerve head (ONH) and posterior displacement of the lamina cribrosa (LC) [2–4]. It also causes retinal thinning in the peripapillary region (PPR), and thusly the measurement of retinal thickness by optical coherence tomography has become an important criterion for glaucoma diagnosis [4–6]. In addition, recent clinical and experimental studies have reported that the peripapillary choroid is also thinned in glaucoma patients [7–11]. Regarding the sclera, studies have failed to establish a clear link between a decrease in its thickness and the presence of this disease [12–15].

The pathophysiology of glaucoma is closely related to high intraocular pressure levels, which is the main risk factor for developing this disease [2–4]. While the mechanical effect of intraocular pressure (IOP) in the ONH has been previously investigated [16–19], its role in other ocular zones has not been well established. Classically, peripapillary retinal thinning observed in glaucoma patients has been described as atrophy, mediated only by axonal death and without any associated mechanical cause. Therefore, several experimental studies have tried to establish the effect of acute IOP elevation on retinal

* Corresponding author.
E-mail addresses: diannymsm@gmail.com (D.M. Muñoz-Sarmiento), olrodriguezm@unal.edu.co (Ó.L. Rodríguez-Montaño), jdalarconc@unal.edu.co (J.D. Alarcón-Castiblanco), magamboam@unal.edu.co (M.A. Gamboa-Márquez), jpcorredorg@unal.edu.co (J.P. Corredor-Gómez), cjcortesr@unal.edu.co (C.J. Cortés-Rodríguez).
[1] Researcher at Eduardo Arenas Ophthalmology Society, Bogota, Colombia.

https://doi.org/10.1016/j.imu.2019.100185
Received 12 December 2018; Received in revised form 15 April 2019; Accepted 15 April 2019
Available online 25 April 2019

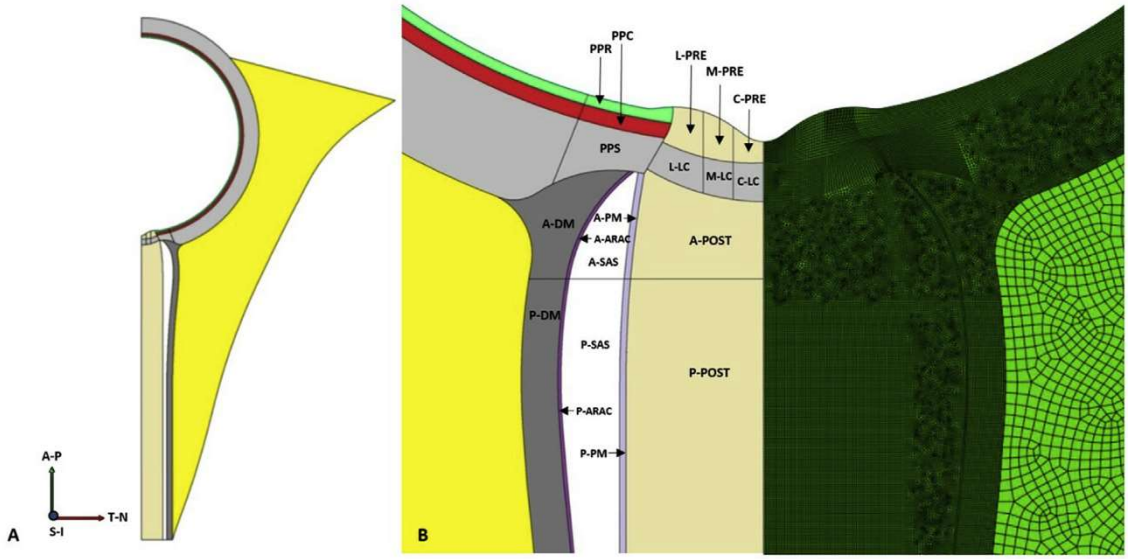

Fig. 1. A. Anatomical configuration. **B.** Biological structures included, and divisions generated. PPR (peripapillary retina), PPC (peripapillary choroid), PPS (peripapillary sclera), PRE (prelaminar tissue), LC (lamina cribrosa), POST (postlaminar tissue), PM (pia mater), SAS (subarachnoid space), ARAC (arachnoid), DM (dura mater), A (anterior), P (posterior), C (central), M (medial), L (lateral).

thickness [20,21].

In this way, Fortune et al. [20] demonstrated that in the rat eye, an acute increase in IOP to 50 mmHg led to peripapillary retinal thinning of 8%, 9% and 11% within the central 10° after 10, 30 and 60 min of IOP elevation, respectively. Similarly, in a non-human primate model, Fortune et al. [21] reported that the retina was 4.8 ± 1.2% thinner after 60 min of acute IOP elevation to 45 mmHg within 800 μm of the ONH centre. Moreover, Wang et al. [11] studied the effect of an acute IOP increase in the choroid in 116 human eyes, finding a decrease in peripapillary choroidal thickness from 177 ± 74 to 169 ± 70 μm with a mean rise in IOP of 10 mmHg.

On the other hand, some clinical and experimental studies have suggested that ONH changes could be caused by prelaminar compression and not by laminar displacement. For instance, Agoumi et al. [22] found greater prelaminar than laminar tissue displacement after acute IOP elevation in glaucoma patients and healthy controls. Additionally, Strouthidis et al. [23] concluded, after an acute IOP increase in five rhesus macaques, that surface compliance changes in the normal monkey ONH primarily reflect prelaminar and peripapillary deformation.

For their part, other studies have pointed out the effect of IOP on the prelaminar region. Reis et al. [24] reported significant acute and chronic prelaminar tissue thickening after surgical IOP reduction in patients with glaucoma. Azuara-Blanco et al. [25] found a significant enlargement in optic disc cupping during acute IOP rise in myopic and non-myopic patients. Furthermore, Fatehee et al. [26] reported greater changes in the LC area than in the prelaminar area in porcine eyes during acute IOP elevation. However, in this last study, when considering only the prelaminar region, greater changes were found in the central prelaminar area than in the peripheral prelaminar areas.

The study of stresses and strains in biological structures is essential to the understanding of biomechanical interactions among tissues. This information is difficult to obtain through experimental techniques due to the impossibility of considering the interaction of all the surrounding tissues, which can alter the results [27]. To overcome this problem, various numerical methods have been used. Among these, the finite element method is currently the most widely employed [27].

In this way, and due to the importance of IOP in the development of glaucoma, several models of the posterior region of the eye have previously analysed the stresses and strains within the ONH through the finite element method [28–35]. Sigal et al. [29] found that the greatest ONH strains were located in the LC. Despite this, to date, the biomechanics of the PPR have received much less attention [34].

Similarly, eye models have not included all meninges, and the majority have not included the subarachnoid space (SAS). Only recently published studies have included the SAS and dura mater [28,31,33–35]; Nevertheless, in these reports, the SAS was only modelled with cerebrospinal fluid pressure (CSFP), whereby its damping function was not taken into account. The biomechanics of the optic nerve meninges have also been little investigated.

In the present study, the primary goal was to evaluate the acute effect of IOP and CSFP on the stresses and strains on the different anatomical structures of the posterior region of the eye. Additionally, the displacements of some structures were also evaluated. As a final step, in this paper, investigation of the impact of including the meninges on the ONH and PPR biomechanical response to IOP and CSFP is presented. To that end, two axisymmetric finite element models were built from one anatomical configuration that included all meningeal layers, the prelaminar and postlaminar region of the ONH, the LC and the complete PPR (including the retina, choroid, and sclera).

2. Methods

Values for lumbar CSFP were used instead of optic nerve CSFP data, since measuring the latter is not possible in clinical settings nowadays, and based on the fact that lumbar CSFP is associated with intracranial pressure and the pressure in the optic nerve [36,37]. In addition, CSFP corresponds to that measured in the lateral decubitus position; though, in the intracranial cavity and ocular globe, CSFP decreases, and even falls to sub-zero values, in a standing position [38]. Finally, the CSFP values studied correspond to the normal (5–15 mmHg), hypertension (greater than 15 mmHg), and hypotension (lower than 5 mmHg) ranges; in this paper, severe intracranial hypertension and hypotension values, reported in the clinical setting, have also been considered [39,40].

2.1. Geometrical details

From the anatomical configuration, two finite element models were generated, one considering the SAS as a solid (model 1), and the other

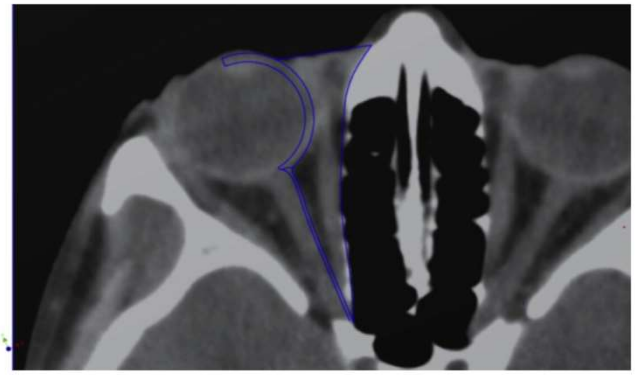

Fig. 2. Axial computed tomography of left eye. The boundaries of the eye globe, the optic nerve, and the bony margins of the orbit were manually delineated from the CT scan.

considering the SAS as an empty space with the CSFP inside it (model 2, explained later). This anatomical configuration was a reconstruction of the orbital cavity based on data from the medial region of the left eye of an orbital CT (computed tomography) image in a healthy female patient (Figs. 1 and 2), as well as on data obtained from the literature, clinical studies, previous models of the ONH, and from an optical coherence tomography (OCT) of the patient's left eye [7,29,41–50]. In this work, extreme population values were avoided. Central retinal vessels were not considered, due to the lack of symmetry in their orbital cavity trajectory and, as earlier studies have pointed out, the weak effect of simplified central retinal vasculature on ONH mechanics [28,29]. Thus, the eye was modelled to have a spherical shape, with the posterior segment opened in its central region, from which the ONH emerged. In turn, this spherical shape was adjusted to the left eye dimensions from the CT scan.

Retinal thickness was constant in all regions (101 μm; patient's value reported from OCT), excluding the zone close to the optic disc where its thickness increased, while the choroid had the same thickness in all zones. Scleral thickness varied along the peripapillary and posterior region in accordance with the experimental data reported by Vurgese et al. [42] (from 0.39 mm at the peripapillary scleral flange to 0.94 mm in the posterior region).

The prelaminar region included ONH excavation, which was modelled based on one of the geometric models proposed by Xu et al. [43]. However, the cup and disc had an idealized circular shape; once the disc and cup radius were located, they were adjusted to achieve a cup/disc ratio equal to 0.39 (patient cup/disc ratio reported from OCT), obtaining a cup radius of 0.34 mm and a disc radius of 0.87 mm [48–50].

The LC was constructed as a section of a spherical shell, with a central thickness of 0.37 mm, in accordance with the experimental data reported by Jonas et al. [47], and a lateral thickness of 0.30 mm [29]. The anterior face of the LC had a radius of 1.9 mm, and a posterior face of 2.15 mm. The postlaminar tissue extended posteriorly from the LC and was covered by the meninges. The pia mater and arachnoid had a constant thickness along the exit of the optic nerve, while the dura mater had a thickness of 0.4 mm and became thicker in the region close to the sclera. For its part, the SAS was thicker in the anterior part and then was progressively thinner, which was in accordance with that reported by Hayreh [45]. The optic nerve extended posteriorly 18.5 mm from the scleral canal.

Furthermore, to achieve a more detailed analysis, the prelaminar region was divided into central, medial and lateral areas, and was then extended to the laminar region. Finally, the optic nerve was also subdivided into anterior (1 mm from the scleral canal) and posterior regions (from 1 mm to the optic nerve end in the orbital cavity) [28].

2.2. Mechanical properties

The pia mater, SAS, arachnoid, fat orbital tissue, retina, choroid, LC, prelaminar and postlaminar tissue were assumed to be isotropic, linear elastic and homogeneous, as defined by the Young's modulus and Poisson's ratio [29,51–53]. In this study, these tissues were considered almost incompressible. Even if these tissues do not show such an ideal behaviour, this type of modelling was chosen due to a lack of information, especially for human species.

The retina and choroid were modelled using an intermediate Young's modulus value from the report by Chen et al. [52]. This was done for two primary reasons: first, the values reported in the vertical and horizontal directions for these structures were similar and without statistically significant differences; and second, to date, this is the only study that has evaluated human posterior ocular tissues in physiological conditions. Posterior sclera was also modelled from the report by Chen et al. [52], based on data describing the stress-strain response of this structure.

The peripapillary sclera is anisotropic tissue, in which the fibrils follow a circular path ringing the scleral canal [54]. In this respect Downs et al. characterized the viscoelastic material properties of peripapillary sclera from the four quadrants surrounding the optic nerve head in normal rabbit and normal monkey eyes, as well as in early-glaucoma monkey eyes [54,55], detecting no quadrants significant differences within each group and postulating that uniaxial testing of tensile specimens obtained tangent to the scleral canal (direction of main fibril orientation) should give valid estimates of its material properties. Data describing the stress-strain curve of peripapillary and posterior sclera were digitized and fit to hyperelastic models with a polynomial strain energy function using $n = 2$ and $n = 3$, respectively. Thus, taking into account the non-linear behaviour of these tissues.

SAS modelling is complex due to the abundance of trabeculae in this space, which stretch from the arachnoid to the pia mater. The space among the trabeculae is filled with cerebrospinal fluid that results in solid–fluid interaction and helps damp and stabilize the movement of the nervous tissue to external loads [53,56,57]. In addition, the pressure effect of cerebrospinal fluid is also present. Previous studies of eye biomechanics have only modelled the SAS as an empty space with CSFP inside of it [28–35]; the shortcoming of this approach is that the SAS damping function is not considered.

Thus, as an initial approach for this work, the SAS damping effect and the CSFP were modelled separately. In model 1, the SAS was assumed to be a solid, which reflects the mechanical role of the cerebrospinal fluid and the trabecular structure of the SAS, and thus taking into account its damping function. Such a model was based on a previous study by Saboori et al. [53], which evaluated the most proper way to model the SAS (fluid, solid or porous media). These authors concluded that the three material models are equally appropriate. To simplify, in this research, the SAS was considered a soft solid, with a Young's modulus of 0.0015 MPa and a Poisson ratio of 0.48, which are the values recommended by Saboori et al. [53]. In model 2, the SAS was considered to be an empty space with CSFP inside it.

Similarly, with an absence of data for the arachnoid, both in the optic nerve and in other anatomical regions, the same Young's modulus value was assumed for the pia mater. This was based on the fact that both meninges are thin membranes with a similar composition of loose connective tissue and squamous epithelial cells; both are derived from the same single layer of mesenchyme surrounding the brain, corresponding the pia mater to the visceral layer, and the arachnoid to the parietal [44]. Therefore, the Young's modulus value for both structures should be close.

Finally, since no mechanical data is available to date for either the human optic nerve dura mater or for other species, the dura mater for this study was modelled after a hyperelastic model with Yeoh strain energy function from data of porcine uniaxial tensile stress that was previously reported by Wang et al. [31]. Table 1 summarizes the

Table 1
Mechanical properties assigned to the tissues.

Structure	Specie	Constitutive model	Properties (MPa)	Reference
Retina	Human	Linear elastic	E = 0.015, v = 0.49	52
Prelaminar tissue	Estimated data	Linear elastic	E = 0.03, v = 0.49	29
Postlaminar tissue	Estimated data	Linear elastic	E = 0.03, v = 0.49	29
Lamina cribrosa	Estimated data	Linear elastic	E = 0.3, v = 0.49	29
Choroid	Human	Linear elastic	E = 0.375, v = 0.49	52
Posterior sclera	Human	Polynomial n = 3	C10 = 3.899256188E-02, C01 = 0, C20 = 0.755668054, C11 = 0, C02 = 0, C30 = −0.4686382, C21 = 0, C12 = 0, C03 = 0, D1 = 0, D2 = 0, D3 = 0	52
Peripapillary sclera	Monkey	Polynomial n = 2	C10 = −308.680057, C01 = 317.583646, C20 = 46014.2168, C11 = −102574.556, C02 = 57590.3243, D1 = 0, D2 = 0	54
Pia mater	Estimated data	Linear elastic	E = 3, v = 0.49	29
Arachnoid	Estimated data	Linear elastic	E = 3, v = 0.49	-
SAS	Estimated data	Linear elastic	E = 0.00115, v = 0.48	53
Dura mater	Porcine	Yeoh	C1 = 0.1707, C2 = 4.2109, C3 = −4.9742	31
Peri orbitary fat tissue	Human	Linear elastic	E = 0.0083, v = 0.49	51

mechanical properties that were assigned.

2.3. Boundary conditions, loads involved and contacts among tissues

The ocular globe was surrounded by adipose tissue, except in the exposed part of the eye, where a pressure of 0 mmHg was applied. A rigid support was placed on the exterior surface of the adipose tissue, simulating the orbital bone. Besides that, the optic nerve was fixed at the orbital canal level in accordance with the optic nerve attachment by fibrous tissue bands in this anatomical region [45]. Finally, based on previous studies, all tissues were tied together at their interface [31,58], excluding between the ocular globe and the adipose tissue, where a frictionless contact was employed. This type of contact helped simulate the Tenon's capsule space, which facilitates ocular motility [59].

Models 1 and 2 were subjected to 12 ocular pressures corresponding to normal (10–20 mmHg), hypotension (lower than 10 mmHg) and hypertension ranges (greater than 20 mmHg). Model 2 was simultaneously subjected to a fixed CSFP of 10 mmHg (normal CSFP).

2.4. Numerical details

The geometry was created using Autodesk Inventor Professional® CAD software. Once created, it was imported to Abaqus®, where the different properties, interactions, boundary conditions and loads previously described were established. Since axisymmetric models in Abaqus are represented as two-dimensional models, isoparametric four-node axisymmetric elements were used in both models. The approximate element size was 100 μm in the peri-orbital fat tissue region and was 20 μm in the other regions. Model 1 included about 175,000 elements and model 2 included about 160,000.

Once the solution process was completed, the mean strains, stresses and displacements for the different structures in the temporal–nasal (T-N), anterior–posterior (A-P) and superior–inferior (S-I) axes, as well as the mean strains and stresses in the principal directions, were obtained. This was because the mean better reflects global damage to the biological structures than the maximum values, with the consequent decrease of overall function and generation of disease; as the functional reservation of tissues protects the global function of localized damage by peak stresses and strains. Only the most relevant results are presented.

3. Results

The results for raising the IOP from 15 to 45 mmHg are presented. More dynamic results are shown further. The results presented correspond to the T-N, A-P and S-I axes. This approach allowed a better comparison of behaviour among the biological structures and correlation to the anatomical planes, experimental studies and clinical research. It was also a necessary approach, as the direction of the principal strains varied considerably among the different tissues studied, and even from point to point within the same tissues (data not shown). Even so, the maximum principal strain, which reflects the maximum strain of each of the structures, is also presented.

In addition, the anterior region (1 mm) showed greater strains ($p = 0.258$, Mann–Whitney U test) and stresses ($p = 0.707$, Mann–Whitney U test) than the posterior region (strain values were on average 45 times greater and stress values were on average 59 times greater; data not shown). This was to be expected, since under pressure, the proximal structures are directly exposed, and therefore, show greater deformations and stresses than the distal ones. Consequently, only the findings corresponding to the anterior region are presented. Some of the statistical results are presented in the form of mean ± standard deviation, range: minimum-maximum value.

3.1. Strains

When analysing only the PPR, the highest strains occurred in the retina. In the retina and choroid, A-P strains were greater than those for T-N and S-I, and in this axis, these tissues were mainly compressed. On the contrary, the peripapillary sclera presented its highest strains on the S-I axis, in which it experienced mainly extension.

In the ONH (LC, prelaminar and postlaminar tissue), the greatest strains were found in the prelaminar region. Same as above, A-P strains in the ONH were greater than T-N and S-I strains, except for the lateral laminar region, where S-I strains were greater. In addition, ONH structures were also compressed on average in the A-P axis, unlike in the T-N and S-I axes. These results suggest that the A-P axis is probably the most important of the anatomical axes for the PPR and ONH, as a result of greater strain values and because in this anatomical axis the tissues experience mainly compression.

By analysing the ONH subzones, the LC showed decreasing strains from the central to the lateral region for T-N, A-P, and S-I axes. The prelaminar region also showed decreasing strains from the central to the lateral region for A-P and S-I axes; however, for the T-N axis, the highest strains were located in the medial prelaminar area. When considering the maximum principal strain, the lateral and medial areas had the highest value in the prelaminar region and LC, respectively.

When considering only the SAS and the meninges, strains were greatest in the SAS, followed by the dura mater and arachnoid. For the SAS and pia mater, the strains in the T-N axis were greater than in the A-P and S-I axes, whereas for the arachnoid and dura mater, S-I strains were greater than in the A-P and T-N axes.

When analysing global results, the peripapillary retina showed the highest strain levels, followed by the prelaminar tissue and the LC, peripapillary choroid, postlaminar tissue and SAS, respectively. When also including subzones in the analysis, the peripapillary retina and

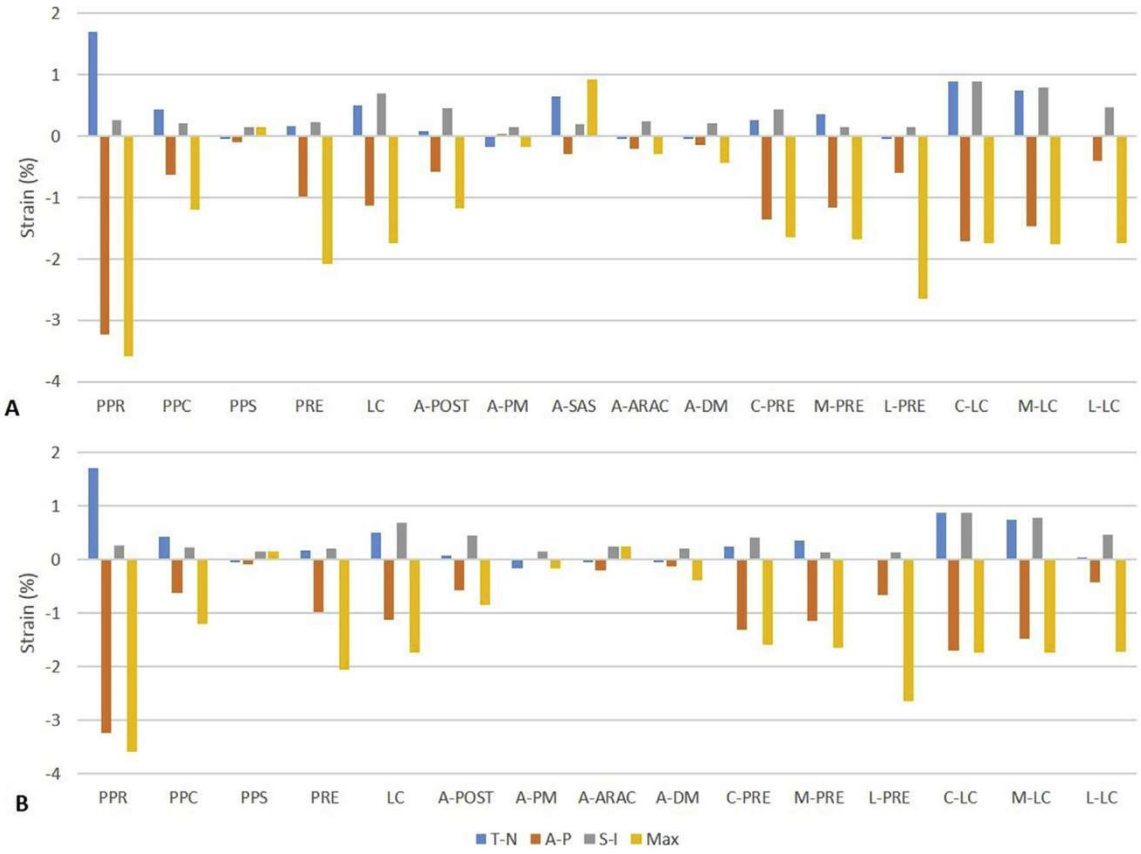

Fig. 3. Computed strains in the T-N, A-P and S-I axes and the maximum principal strain (Max) for each biological region in model 1 (A) and 2 (B), due to an IOP increase from 15 to 45 mmHg. A positive value indicates extension; a negative value indicates compression.

lateral prelaminar region presented the highest maximum principal strain values, and the peripapillary retina and central laminar region showed the highest A-P strain levels (Fig. 3).

Previous results were consistent for both models, with little difference between models that had a solid or an empty SAS. Therefore, modelling of the SAS as a solid or an empty space with the CSFP inside it did not significantly change these results ($p = 0.845$, Mann–Whitney U test).

3.2. Von Mises stress (distortion energy)

Von Mises stress is the equivalent of distortion energy. In turn, distortion energy represents the work transmitted to the tissues to change their shape. In the models, the Von Mises stresses were much lower in the structures composed only of nervous tissue (retina, prelaminar and postlaminar tissue) than in the other regions ($p = 0.000$, Mann–Whitney U test). The SAS also showed low Von Mises stress levels (Fig. 4).

3.3. A-P displacements

A-P displacements have been studied in the ONH and PPR in different clinical and experimental research [16–20,22,23]. Therefore, these displacements in the ONH, choroid, and retina were investigated. The greatest displacements were found in the peripapillary choroid, followed by peripapillary retina, postlaminar tissue, prelaminar tissue and LC, with posterior displacements only in the prelaminar tissue. Nevertheless, computed A-P displacements in the subzones revealed posterior displacements in the laminar and prelaminar central and medial area, as well as anterior displacements in the lateral region of the prelaminar tissue and LC (Fig. 5). Modelling of the SAS as a solid or an empty space with CSFP inside of it did not significantly change the results ($p = 0.429$, Mann–Whitney U test).

3.4. Influence of IOP

In order to have a better approach for the effect of IOP in dynamic conditions, a subsequent analysis was carried out. The IOP was varied for a total of 12 ocular pressures (5, 10, 15, 20, 25, 30, 35, 40, 45, 50, 55 and 60 mmHg), the absolute strain values for all the structures at each IOP were obtained, and a linear regression was performed to produce the slope that describes the strain change over a given IOP change. An excellent linear correlation was obtained for all the biological structures of model 1 ($R^2 = 0.989 \pm 0.014$, range: 0.911–0.996; $p = 0.001 \pm 0.004$, range: 0.029–0.000) and model 2 ($R^2 = 0.990 \pm 0.033$, range: 0.755–1.000; $p = 0.001 \pm 0.004$, range: 0.031–0.000).

In model 1, all the biological regions showed increments in linear and proportional strain with a rise in IOP, except for the T-N axis in the laminar and prelaminar lateral region (Fig. 6). In model 2 most of the structures showed linear increments in their strains on elevating the IOP. Nevertheless, some others exhibited strain decrements or mixed behaviour (strain increments and decrements when increasing the ocular pressure, depending on the IOP range) (Fig. 7). Thus, the postlaminar tissue presented mixed behaviour, and a change in its mechanics at high ocular pressures; with an increased compression in the A-P axis and an increased extension in the other axes at high IOP levels, and a decreased compression in the A-P axis and decreased extension in the T-N and S-I axes at low IOP levels (Fig. 8). The anatomical regions with the highest slopes for IOP changes were the peripapillary retina, the prelaminar tissue and the LC.

In addition, in a similar experiment, A-P displacements at each IOP were obtained, and a linear regression with the absolute values was carried out. Most of the structures had increments in their

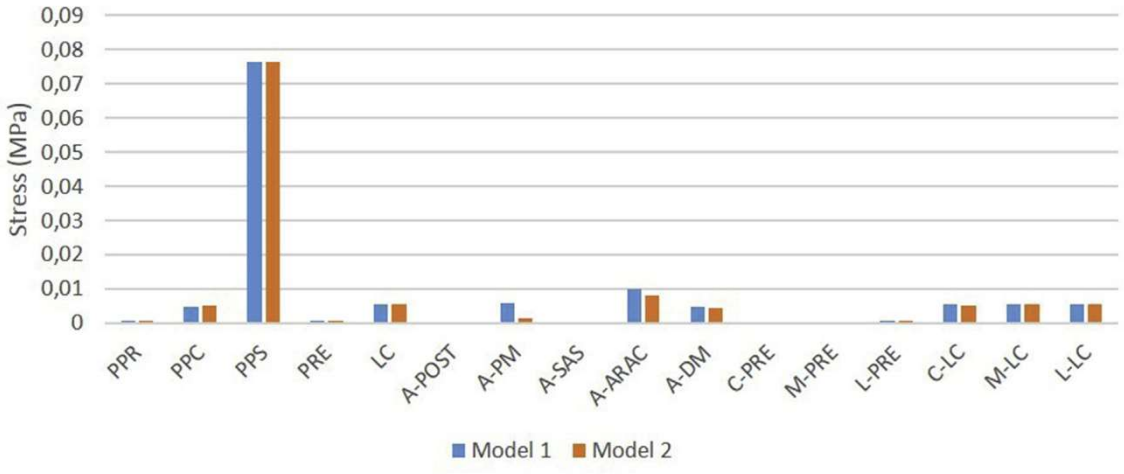

Fig. 4. Computed Von Mises stresses for each anatomical region in model 1 and 2, due to an IOP increase from 15 to 45 mmHg. Low values of the retina, prelaminar and postlaminar tissue can be observed (p = 0.000, Mann-Whitney *U* test).

displacements with a rise in IOP. The LC initially showed a posterior displacement and then an anterior displacement (Figs. 8 and 9).

3.5. Influence of CSFP

Glaucoma has been associated with low CSFP levels, and translaminar pressure (the IOP minus the CSFP) has been suggested as a better predictor of the disease than the IOP alone [60,61]. To test this, the effect of decreasing the CSFP from 11 to 3 mmHg were investigated, while the IOP was fixed at 45 mmHg. Postlaminar tissue showed the highest levels of strain, followed by the pia mater, LC and prelaminar tissue, respectively. Inside the PPR, the retina was the most deformed layer, with the highest strains in the T-N axis. For its part in the ONH, A-P strains were greater than in the other anatomical axes, with compression of the postlaminar tissue and LC, and extension of the prelaminar region. When considering the ONH subzones, the highest strains were located in the lateral prelaminar region; despite this, the central and medial region of the LC experienced the greatest levels of strain in the A-P direction (Fig. 10).

Regarding A-P displacements, the retina, choroid, sclera and LC presented an anterior displacement, unlike prelaminar tissue, which showed a posterior displacement. However, the analysis of the subzones revealed that the central and medial regions of LC and prelaminar tissue experienced a posterior displacement, in contrast to the lateral regions, which showed an anterior displacement (Fig. 11).

In an additional experiment, model 2 was submitted to an IOP of 45 mmHg, and the CSFP was varied for a total of 20 CSFP values (0.125, 0.25, 0.5, 1, 3, 5, 7, 9, 11, 13, 15, 17, 19, 21, 23, 25, 30, 35, 40 and 45 mmHg). Then, the strains for all the structures at each CSFP were obtained, and a linear regression was performed with the absolute values to obtain the slope describing the strain change over a CSFP change. An excellent linear correlation was obtained ($R^2 = 0.983 \pm 0.039$, range: 0.811–0.999; $p = 0.000 \pm 0.0002$, range: 0.002–0.000).

As can be seen in Fig. 12, some biological structures showed increments in their strains by raising the CSFP, while some showed decrements and a third group showed mixed behaviour, depending on the CSFP values. This was the case for the postlaminar tissue, which was the structure most affected by the CSFP variations. In this manner, when the CSFP was higher than or equal to 15 mmHg, the S-I axis showed compression, and extension for inferior values; similarly, when the CSFP was greater than or equal to 3 mmHg the T-N axis presented compression, with extension for lower values. The A-P axis showed extension when the CSFP was greater than or equal 13 mmHg, and compression for inferior CSFP values. Thus, the biomechanical behaviour of the postlaminar tissue at low CSFP values was similar to that obtained at high ocular pressures; likewise, the biomechanical behaviour at high CSFP values was very similar to that obtained at low ocular pressures, indicating that a low CSFP in combination with a high IOP, or a high CSFP in combination with a low IOP, produces a synergistic mechanical effect on the postlaminar tissue (Fig. 8).

Moreover, there was an increment in prelaminar tissue strains upon CSFP elevation (with the exception of the maximum principal strain), unlike that of the LC, for which there was an increment in strains when

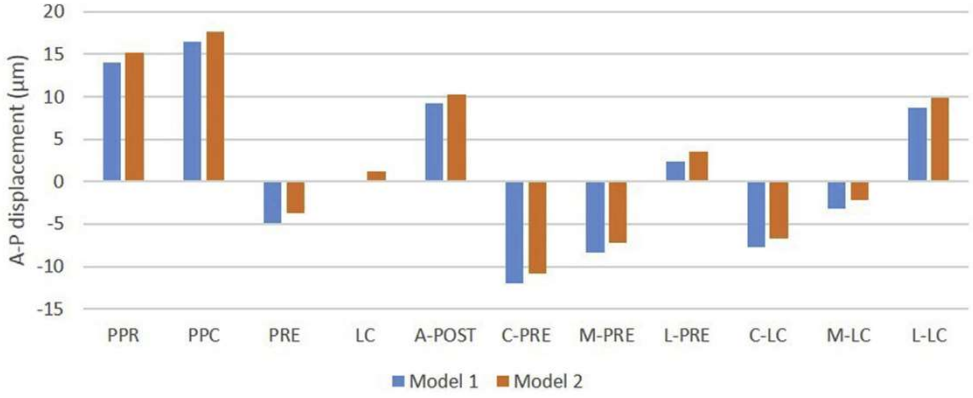

Fig. 5. Computed A-P displacements for each anatomical region in model 1 and 2, due to an IOP increase from 15 to 45 mmHg. A positive value indicates an anterior displacement, and a negative value indicates a posterior displacement.

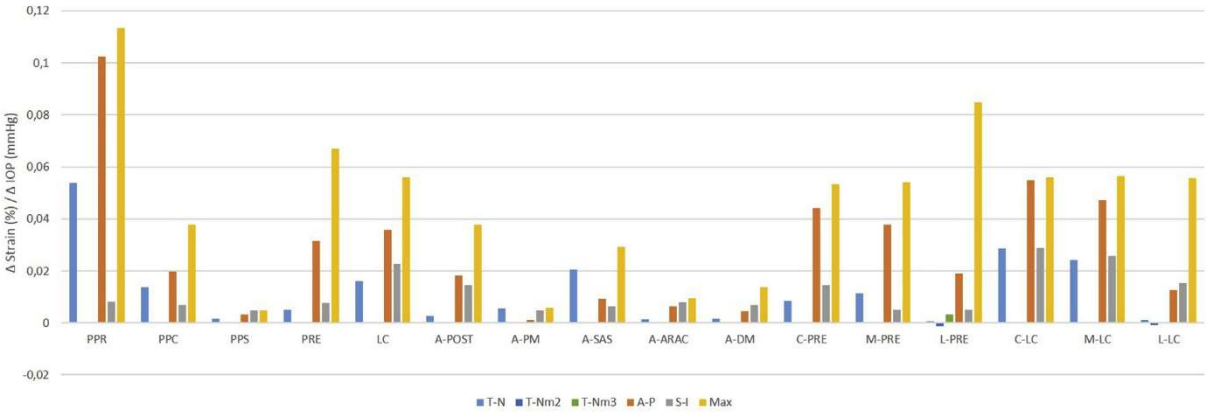

Fig. 6. Change in the T-N, A-P and S-I strains and the maximum principal strain (Max) over the IOP change in model 1. The graphic shows the slope obtained for each of the biological structures. A positive value indicates increased strain due to an elevated IOP, and a negative value indicates increased strain due to a decreased IOP. The structures with only T-N, A-P, S-I or Max indicate a single behaviour; structures including m3 and/or m2 indicate a mixed behaviour, depending on the IOP range. PRE-L: T-N = 5–10 mmHg, T-Nm2 = 20–35 mmHg, T-Nm3 = 35–60 mmHg. LC-L: T-N = 5–30 mmHg, T-Nm2 = 30–60 mmHg.

decreasing the CSFP. When considering the subzones, the central and medial LC regions had the most important inversely proportional relationship with the CSFP. The retina and choroid also showed increased strains on decreasing the CSFP.

Lastly, the A-P displacements at each CSFP were obtained, and a linear regression was carried out with the absolute values ($R^2 = 0.944 \pm 0.037$, range: 0.869–0.991; $p = 0.012 \pm 0.045$, range: 0.169–0.000). An incremented anterior displacement by decreasing the CSFP was observed for the retina, choroid and postlaminar tissue; on the contrary, decreasing the CSFP produced an incremented posterior displacement for the prelaminar tissue. The LC presented an incremented anterior displacement for pressures under and over 11 mmHg. When considering only the subzones, the central and medial regions of the LC and prelaminar tissue showed an incremented posterior displacement by reducing the CSFP, with the highest posterior displacements located in the central area of the prelaminar tissue and LC; while the lateral regions of both structures presented an incremented anterior displacement by reducing the CSFP (Figs. 13 and 14). It is noteworthy that the effect of CSFP on A-P displacements was weaker for all the structures when compared to the effect of IOP, save for the LC and the postlaminar tissue; for this last structure, the displacements caused by the CSFP were around twice than the produced by the IOP.

3.6. Influence of the meninges

Although there are different nerves in the human body, the optic nerve is the only one covered by meninges, which gives it a special feature. Despite this, while the function of the meninges and SAS has been studied in the cranial and spinal cavity, its role in the optic nerve has received much less attention. In order to study the impact of each of the meningeal layers and the SAS on the biomechanical response of the ONH and PPR due to fluctuations in IOP, an analysis was conducted in which all meninges were replaced by adipose tissue (thus, simulating a naked optic nerve); subsequently, the meninges were progressively added to the postlaminar tissue.

For the naked optic nerve and for each meningeal layer added, the IOP was varied (5, 10, 15, 20, 25, 30, 35, 40, 45, 50, 55 and 60 mmHg), and the maximum principal strain and A-P strain for each structure was obtained. Then, a linear regression was performed with the absolute values, obtaining the slope that describes the strain change over the IOP change. For this experiment, both model 1 (solid SAS) and model 2 (CSFP) were considered. In model 2, the CSFP was fixed at 10 mmHg. An excellent linear correlation was obtained for all the biological structures when considering the maximum principal strain ($R^2 = 0.996 \pm 0.006$, range: 0.966–1.000; $p = 0.000 \pm 0.000$, range: 0.000–0.000) and the A-P strain ($R^2 = 0.997 \pm 0.003$, range: 0.986–1.000; $p = 0.000 \pm 0.000$, range: 0.000–0.000).

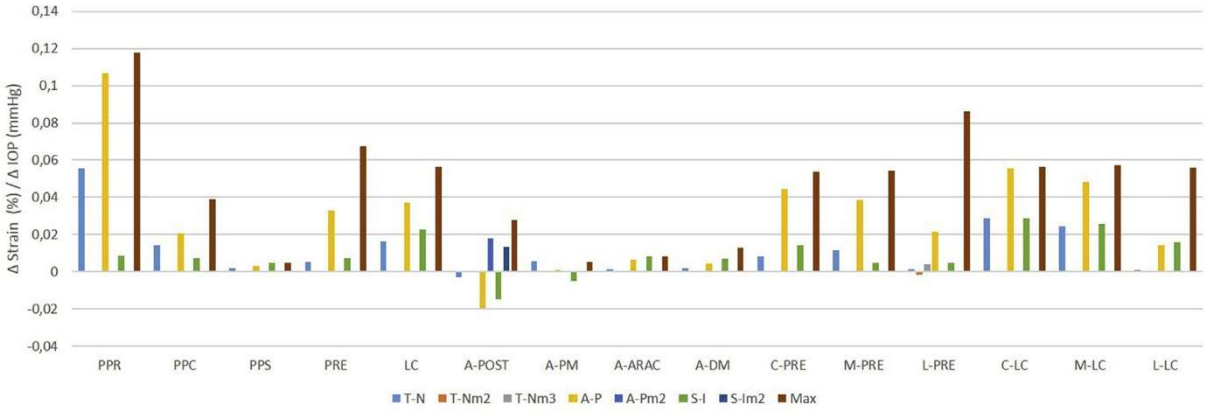

Fig. 7. Change in the T-N, A-P and S-I strains and the maximum principal strain (Max) over the IOP change in model 2. The graphic shows the slope obtained for each of the biological structures. A positive value indicates an increasing strain by elevating the IOP, a negative value indicates an increasing strain by decreasing the IOP. The structures with only T-N, A-P, S-I and Max indicate a single behaviour; structures including m3 and/or m2 indicate a mixed behaviour, depending on the IOP range. PRE-L: T-N = 5–25 mmHg, T-Nm2 = 25–50 mmHg, T-Nm3 = 50–60 mmHg. A-POST: A-P = 5–35 mmHg, A-Pm2 = 35–60 mmHg, S-I = 5–30 mmHg, S-Im2 = 30–60 mmHg.

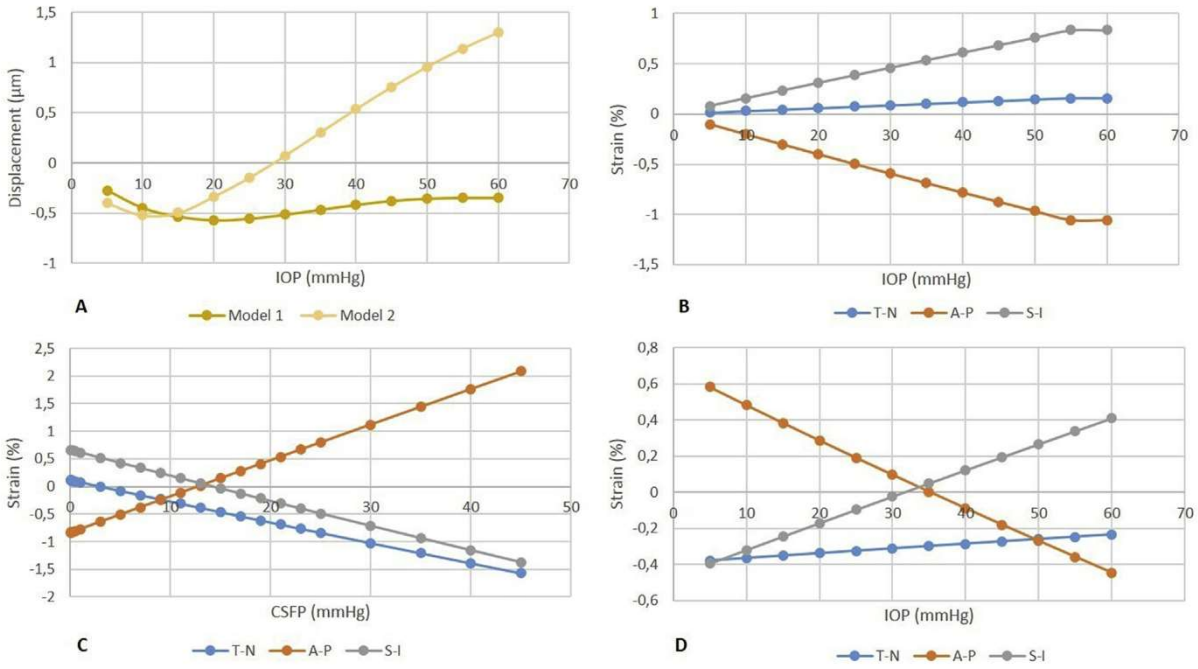

Fig. 8. A-P laminar displacement versus IOP in model 1 and 2 (**A**). An initial posterior displacement that turns into an anterior displacement can be observed. A-POST strains in the T-N, A-P and S-I axes versus IOP in model 1 (**B**) and 2 (**D**). A-POST strains in the T-N, A-P and S-I axes versus CSFP in model 2 (**C**).

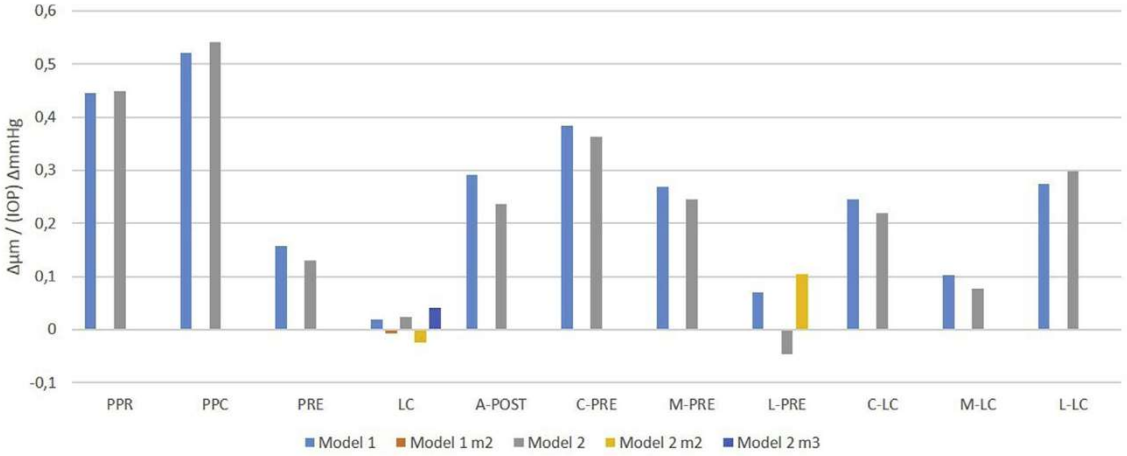

Fig. 9. Change in A-P displacement over the IOP change in model 1 (R2 = 0.981 ± 0.027, range: 0.994–0.909; p = 0.004 ± 0.014, range: 0.04–70.00), and 2 (R2 = 0.949 ± 0.114, range: 0.581–1.000; p = 0.006 ± 0.022, range: 0.078–0.000). The graphic shows the slope obtained for each of the biological structures. A positive value indicates an increasing displacement when increasing the IOP, and a negative value indicates an increasing displacement when decreasing the IOP. The structures that include m3 and/or m2 indicate a mixed behaviour, depending on the IOP range. Model 1, LC: A-P = 5–20 mmHg, A-Pm2 = 20–60 mmHg. Model 2, LC: A-P = 5–10 mmHg, A-Pm2 = 10–30 mmHg, A-Pm3 = 30–60 mmHg. L-PRE: A-P = 5–30 mmHg, A-Pm2 = 30–60 mmHg.

The results revealed that the addition of all the meningeal layers and SAS considerably decreased the strains in the ONH. The postlaminar tissue was the structure with the highest maximum principal strain reduction (−34.53% in model 2 vs. −10.45% in model 1) and A-P strain reduction (−103.03% in model 2 vs. −26.33% in model 1) when compared to the naked optic, followed by the LC (maximum principal strain reduction of −14.75% in model 2 vs. −15.49% in model 1; A-P strain reduction of −12.34% in model 2 vs. −15.71% in model 1), and the prelaminar tissue (maximum principal strain reduction of −10.71% in model 2 vs. −11.54% in model 1; A-P strain reduction of −3.76% in model 2 vs. −7.86% in model 1). Moreover, the pia mater was the layer for which the strains were most reduced in the LC (maximum principal strain reduction of −10.03% and A-P strain reduction of −9.73% in model 1). Additionally, the major reduction in the prelaminar tissue strains was due to the dura mater (maximum principal strain reduction of −1.12% in model 2 vs. −5.04% in model 1; A-P strain reduction of −3.39% in model 2 vs. −7.24% in model 1), and the major reduction in the postlaminar tissue was due to the arachnoid (maximum principal strain reduction of −28.19% in model 2 vs. −1.37% in model 1; A-P strain reduction of −104.93% in model 2 vs. −3.75% in model 1). For its part, addition of the SAS had a low impact on ONH and PPR strains (Fig. 15).

Finally, in a similar analysis, and in order to establish the impact of the dura mater on the biomechanical response to CSFP variations, the dura mater was replaced by adipose tissue in model 2, and then added back. The CSFP was varied (0.125, 0.25, 0.5, 1, 3,7,9,11,13,15, 20 and 25 mmHg), while the IOP was fixed at 45 mmHg. An excellent linear correlation was obtained for maximum principal strain (R^2 = 0.996 ± 0.017, range: 0.915–0.999; p = 0.0001 ± 0.0004, range: 0.002–0.000) and A-P strain (R^2 = 0.989 ± 0.026, range:

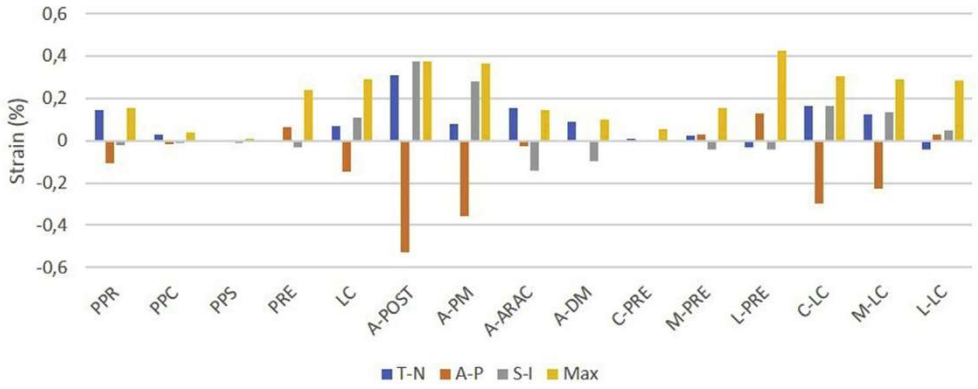

Fig. 10. Computed strains in the T-N, A-P and S-I axes and the maximum principal strain (Max) for each biological region in model 2, due to an CSFP decrease from 11 to 3 mmHg. A positive value indicates extension; a negative value indicates compression.

0.908–0.999; $p = 0.0001 \pm 0.0004$, range: 0.002–0.000). The addition of the dura mater decremented the retinal (maximum principal strain reduction of −6.70% and A-P strain reduction of −7.73%) and choroidal strains (maximum principal strain reduction of −17.06% and A-P strain reduction of −14.40%), as well as incremented scleral strains (maximum principal strain increase of 5.32% and A-P strain increase of 26.82%). For its part, the effect on the ONH was weak. Above results indicate the importance of including all meninges when studying the effects of IOP and CSFP in the posterior region of the eye (Fig. 16).

3.7. Sensitivity study

The stiffness of eye tissues can vary among the population; therefore, a study of the influence of the properties of the meninges, SAS, LC and peripapillary sclera on the maximum principal and A-P strain in the ONH, PPR, SAS and meninges was performed. The IOP was fixed at 45 mmHg, and each factor was increased and decreased by 25% and 50% from the baseline value, except for the peripapillary scleral factors C02, C10 and C11, which were increased by 25% and 50%, and only decreased by 25%. Then, a linear regression was performed with the absolute values, obtaining the strain change per unit change for each of the tissues (Δ Strain (%)/Δ MPa) (maximum principal strain: $R^2 = 0.946 \pm 0.084$, range: 0.584–1.000; $p = 0.086 \pm 0.131$, range: 0.387–0.000; A-P principal strain: $R^2 = 0.942 \pm 0.091$, range: 0.361–1.000; $p = 0.087 \pm 0.135$, range: 0.590–0.000). This data was compared with the IOP and CSFP results previously obtained (Δ Strain (%)/Δ MPa). Variations in IOP, CSFP and SAS stiffness had the strongest influence on strains within the ONH and PPR. The influence of the SAS was especially important for the postlaminar tissue in the ONH, as well as for the meninges (**Supplementary data 1**).

3.8. Results validation

It is important to validate numerical simulations. Model results were compared with data from eight experimental and clinical studies. These studies corresponded only to acute elevations in IOP or CSFP. Qualitative accuracy (adequate prediction of the tissues' response to IOP or CSFP variation) of 95.00% and 83.33% was obtained for model 1 and model 2, respectively. Likewise, to quantitatively validate the models' accuracy, the relative error compared to the experimental and clinical data was calculated. An absolute average of 91.17 ± 75.88% (1.12–340.10) was obtained for model 1, and 95.48 ± 73.87% (2.44–357.61) for model 2 (Tables 2 and 3).

4. Discussion

Various models of ONH have been constructed and analysed using the finite element method; however, those models have not included the complete meningeal layers and the SAS. Furthermore, some eye models assumed that the optic nerve was only covered by the pia mater [29,30,32]. Thus, when obtaining the strain distribution for a model with only the pia mater, the greatest strains are located in the LC (our own study of this model corroborated this statement).

This is in contrast with the results observed in the models presented here, in which the retina and prelaminar tissue had the highest strain values. This is probably due to the fact that the retina and prelaminar tissue are soft structures that are directly exposed to the effect of IOP, which sum to the expansion of the scleral canal and LC by extension stresses, causing high strain levels. Nevertheless, greater strains do not necessarily mean more axonal damage, since the microscopic arrangement, axoplasmic flow and vascular supply has not been considered. In contrast, higher strains imply greater detectable anatomical deformations.

Thus, when considering only ONH strains, the highest maximum

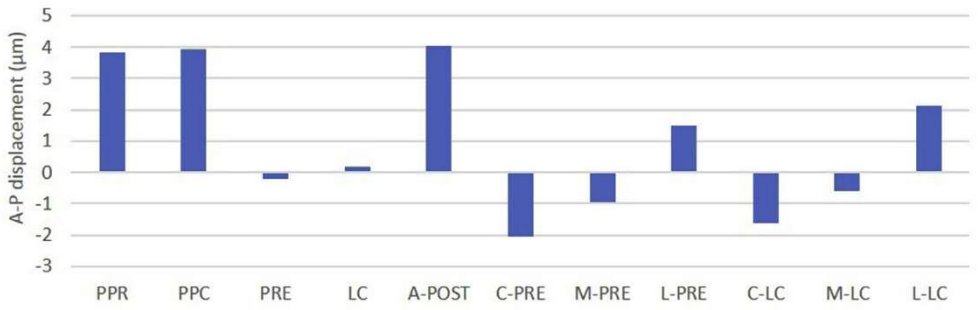

Fig. 11. Computed A-P displacements for each anatomical region in model 2, due to an CSFP decrease from 11 to 3 mmHg. A positive value indicates an anterior displacement, and a negative value indicates a posterior displacement.

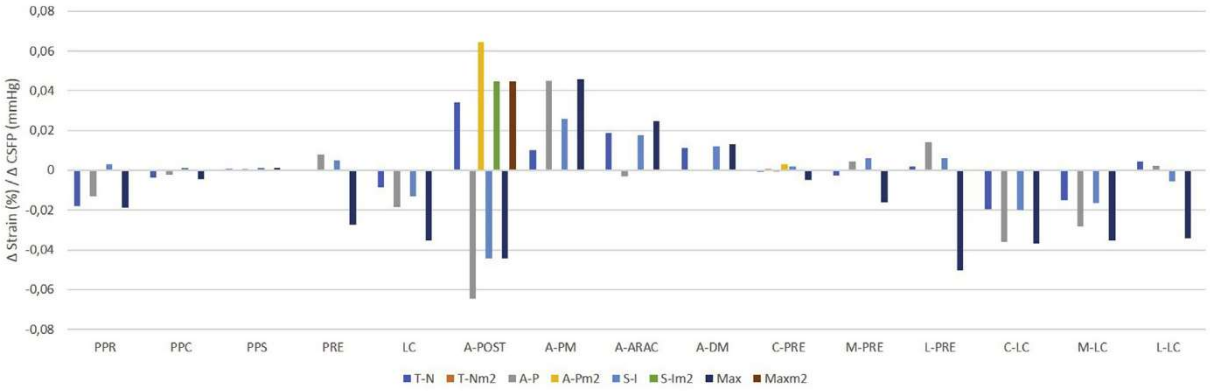

Fig. 12. Change in the T-N, A-P and S-I strains and the maximum principal strain (Max) over the CSFP change in model 2. The graphic shows the slope obtained for each of the biological structures. A positive value indicates an increasing strain caused by elevating the CSFP, and a negative value indicates an increasing strain caused by decreasing the CSFP. The structures with only T-N, A-P, S-I and Max indicate a single behaviour; structures including m2 indicate a mixed behaviour, depending on the CSFP range. C-PRE: T-N = 0.125–23 mmHg, T-Nm2 = 23–45 mmHg, A-P = 0.125–9 mmHg, A-Pm2 = 9–45 mmHg. A-POST: A-P = 0.125–13 mmHg, A-Pm2 = 13–45 mmHg, S-I = 0.125–15 mmHg, S-Im2 = 15–45 mmHg, Max = 0.125–15 mmHg, Maxm2 = 15–45 mmHg.

principal strain values were located in the lateral prelaminar region, not in LC, which had its major deformation in the medial area. Recently, Voorhees et al. [62] studied LC deformations through finite element modelling from sheep histological sections and found that peripheral LC pores had significantly higher strains than central ones. Furthermore, in a human study of regional LC deformations, Midgett et al. [63] reported greater maximum shear strain in the peripheral LC than in the central part; however, they found no significant differences when analysing the maximum principal strain between these regions.

Previous studies have signalled the LC as the primary site of injury in glaucoma [64–66]. It is interesting that when considering only the anatomical axes, the LC was deformed and compressed more than the prelaminar tissue; similarly, when considering only the anatomical directions, inside the ONH, the central region of the LC was deformed and compressed most, followed by the central prelaminar tissue. This means to the authors that probably the axonal damage is more related to the strains in the anatomical axes, and especially in the A-P axis due to its compressive effect, than with the strains in the principal directions, and which emphasizes the importance of also considering the anatomical planes in the ocular biomechanics analysis. Likewise, this means that with a rise in IOP, one of the most remarkable clinical alterations would be an increment of ONH excavation.

On the other hand, the PPR has been minimally explored. As this region also suffers significant morphological changes in glaucoma patients, the study of its biomechanics is of great importance. During IOP elevation, all of the PPR layers would show thinning; notwithstanding, the retina would be most affected, exhibiting the greatest values of thinning and deformation. On the contrary, choroidal and scleral thinning would be much lower.

Classically, peripapillary retinal thinning seen in glaucoma patients has been described as atrophy, mediated only by axonal death at the LC and without any associated mechanical cause. To test this, several studies have used human and non-human models in which the IOP has been raised acutely, finding a small percentage decrease in peripapillary retinal thickness [20,21]. Additionally, a small degree of thinning has also been reported for the choroid in acute IOP elevations [11].

In this research, similar thinning percentages were obtained for both structures, especially for the retina. However, considering the biomechanical properties of the three layers of the eye, it can be suspected that this thinning behaviour could be present in the whole ocular area and not only in the PPR. In fact, choroidal thinning has also been documented in the macular area when the IOP is acutely elevated [11].

In this manner, during an increase in IOP, it can be expected that the entire retina would be submitted to compression forces that would cause thinning in its whole structure. Because the whole retina accounts for a great ocular area and sum, the retina reaches its plastic phase very fast [67]; this small percentage of retinal thinning could imply a more significant mechanical effect that, coupled with the damage suffered in the ONH, could contribute to the cell apoptosis and retinal atrophy observed in glaucoma. This must be tested in future experimental and finite element studies.

In addition, since the entire retinal thickness, rather than just the

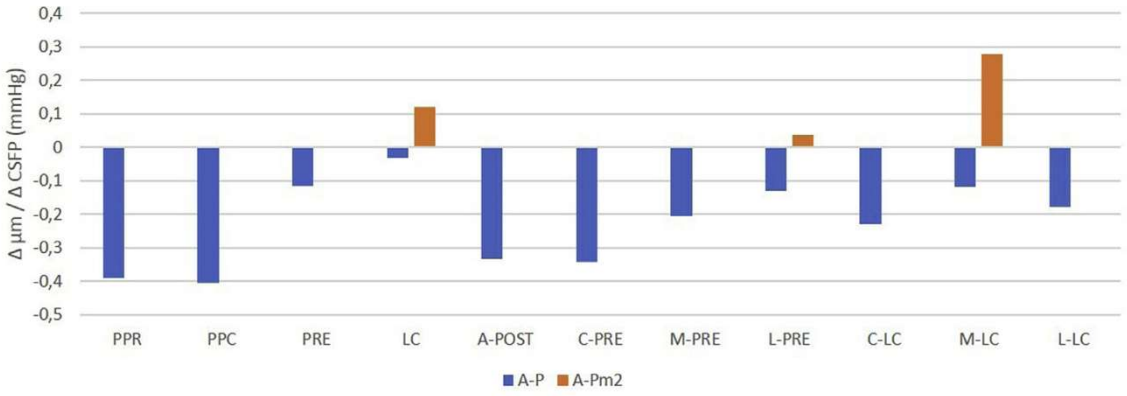

Fig. 13. Change in A-P displacement over the CSFP change in model 2. The graphic shows the slope obtained for each of the biological structures. A positive value indicates an increasing displacement caused by elevating the CSFP, and a negative value indicates an increasing displacement caused by decreasing the CSFP. The structures including m2 indicate a mixed behaviour, depending on the CSFP range. LC: A-P = 0.125–11 mmHg, A-Pm2 = 11–45 mmHg. M-LC: A-P = 0.125–30 mmHg, A-P m2 = 30–45 mmHg. L-PRE: A-P = 0.125–35 mmHg, A-P m2 = 35–45 mmHg.

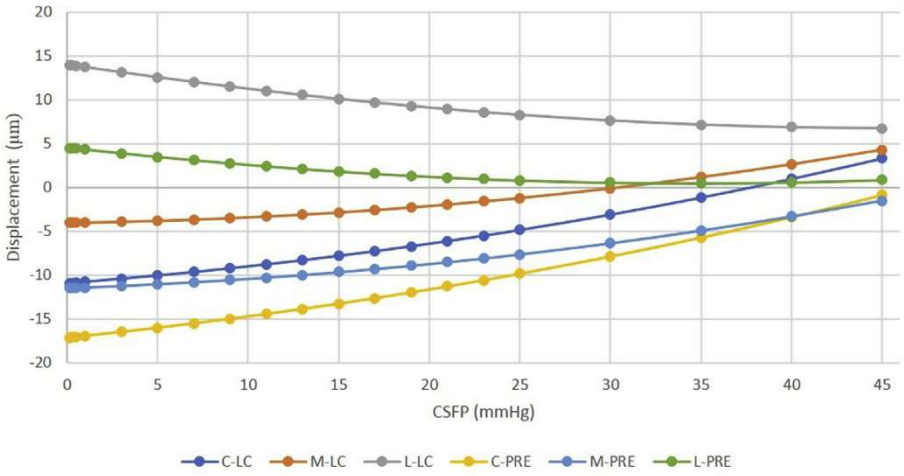

Fig. 14. A-P laminar displacements versus CSFP in model 2.

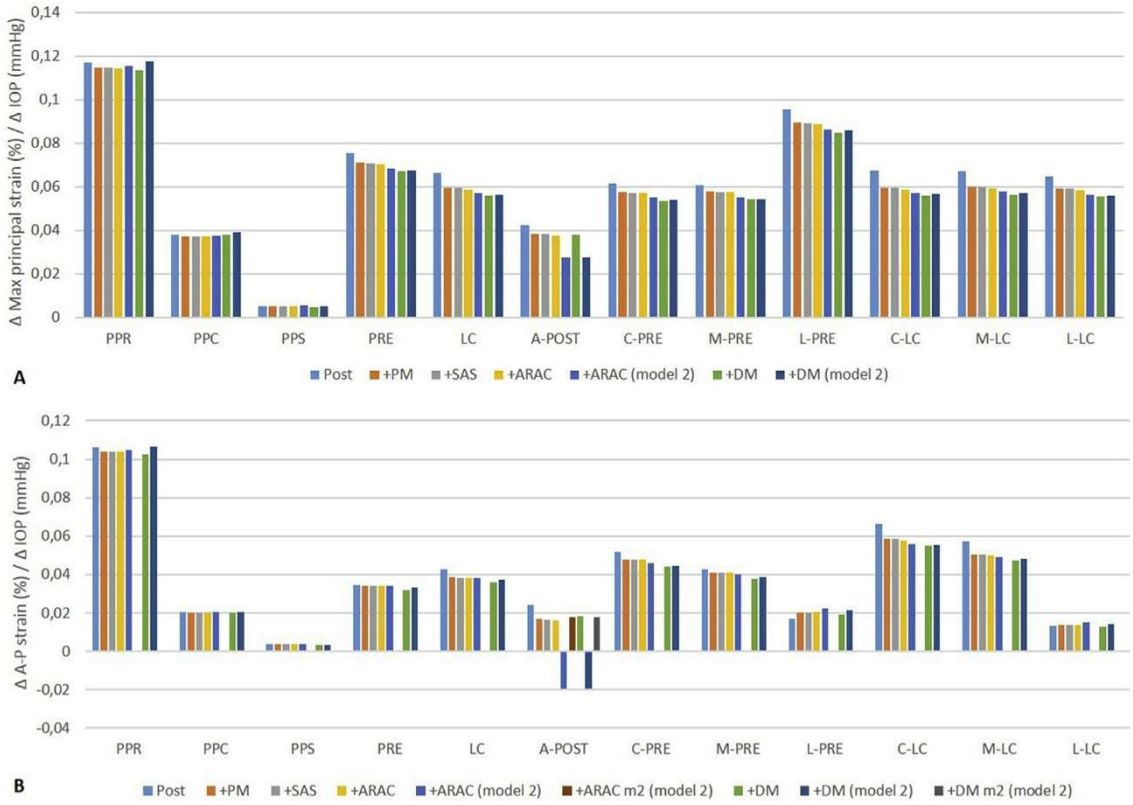

Fig. 15. Maximum principal strain (**A**) and A-P strain (**B**) over the IOP change for each added meningeal layer. The graphic shows the slope obtained for each of the biological structures. A positive value indicates an increasing strain caused by elevating the IOP, and a negative value indicates an increasing strain caused by decreasing the IOP. The structures including m2 indicate a mixed behaviour, depending on the IOP range. +ARAC (model 2), A-POST: A-P = 5–35 mmHg, A-Pm2 = 35–60 mmHg. +DM (model 2), A-POST: A-P = 5–35 mmHg, A-Pm2 = 35–60 mmHg.

retinal nerve fibre and ganglion cell layers, are subjected to compression forces, mechanical compression could also affect outer retinal layers (which do not suffer mechanical damage at the ONH level), leading to an injury in this region. This could produce the outer retinal damage observed in some studies [68,69], and also needs to be tested in the future.

For another part, the variations in IOP produced more strains in the PPR, LC and prelaminar tissue than CSFP changes (greater slope), confirming the major role of IOP in glaucoma. However, variations in CSFP had a greater effect on the postlaminar tissue than IOP changes. So, intracranial hypertension would primarily compromise this anatomical structure, with increased compression in the T-N and S-I axes, which would probably lead to a subsequent blockage of circulatory flow and papilledema. This is in line with the experimental research of Feola et al. [70], who reported that an acutely elevated CSFP mainly correlated positively with increasing postlaminar tissue strains.

Moreover, based on our results, it can be predicted that ocular hypotony would facilitate the establishment of papilledema by means of increased T-N and S-I postlaminar compression. This, in fact, has been previously described by Faingold et al. [71], who reported papilledema after trabeculectomy in a patient with pseudotumor cerebri. Also, Greenfield et al. [72] described a case of papilledema that was seen

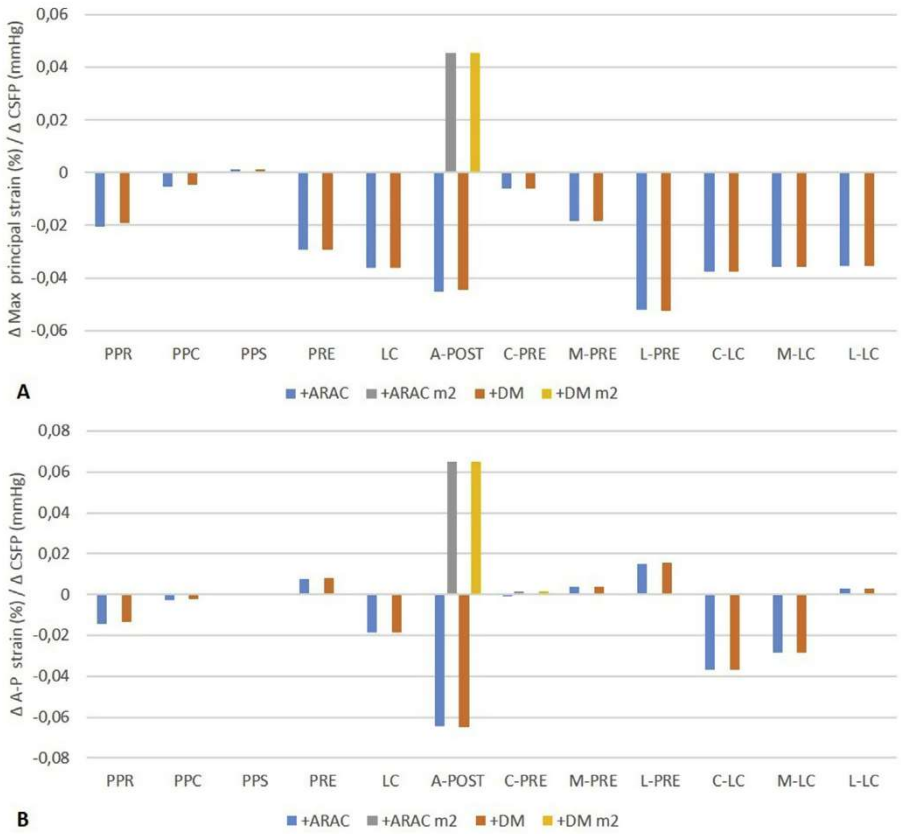

Fig. 16. Maximum principal strain (**A**) and A-P strain (**B**) over the CSFP change in a model without dura mater (+ARAC), and with the addition of dura mater (+DM). The graphics shows the slope obtained for each of the biological structures. A positive value indicates an increasing strain caused by elevating the CSFP, and a negative value indicates caused an increasing strain by decreasing the CSFP. The structures including m2 indicate a mixed behaviour depending on the CSFP range. +ARAC, A-POST: A-P = 0.125–13 mmHg, A-Pm2 = 13–25 mmHg, Max = 0.125–15 mmHg, Maxm2 = 15–25 mmHg. C-PRE: A-P = 0.125–9 mmHg, A-Pm2 = 9–25 mmHg. +DM, A-POST: A-P = 0.125–13 mmHg, A-Pm2 = 13–25 mmHg, Max = 0.125–15 mmHg, Maxm2 = 15–25 mmHg. C-PRE: A-P = 0.125–9 mmHg, A-Pm2 = 9–25 mmHg.

unilaterally following trabeculectomy in a patient with pseudotumor cerebri.

In contrast, the higher risk of developing glaucoma in patients with low CSFP could be due to an augmentation in peripapillary retinal, choroidal and LC central and medial thinning; to a change in postlaminar mechanics, as well as because of incremented posterior displacement of the prelaminar and laminar central and medial regions. Yang et al. [73] examined the effect of chronically lowering the CSFP on the optic nerve and retinal nerve fibre layer in four monkeys; two of the four monkeys showed a bilateral reduction in retinal thickness and neuroretinal rim area and volume, as well as an increased cup/disc ratio. Garcia-Montesinos et al. [74] evaluated 12 patients with intracranial hypertension before and after lowering the CSFP and found that reduced CSFP was associated with retinal fibre layer thinning, prelaminar thinning and backward movement of the LC. In addition, Lee et al. [75] showed that greater translaminar pressure was associated with greater LC central depth, but not with superior, inferior and mean LC depth in healthy human eyes. Based on those results, Lee et al. [75] speculated that the interaction between IOP and CSFP was mainly centred in the central region of the optic nerve. The results presented here are consistent with most of these findings.

Finally, addition of the meninges produced a reduction in ONH strains due to IOP changes, and dura mater inclusion decremented peripapillary retinal and choroidal strains to CSFP variations, demonstrating that the function of the meninges in the optic nerve is not only that of a protective cover, but also that they have an important mechanical function in modifying the biomechanical response to the different external forces that act on the posterior segment of the eye, and consequently affecting the strains in both the ONH and PPR.

Contrary to expectations, addition of the SAS did not reduce ONH and PPR strains due to IOP fluctuations. Nevertheless, variation of its properties had a great impact on ONH and PPR strains. Based on this, it can be predicted that SAS stiffness would have a great influence on axonal damage in patients with glaucoma. The SAS could also protect the delicate nervous tissue of the optic nerve from high strain levels during ocular trauma and ocular movements, which would agree with the SAS damping function against external forces that was previously described for the cranial region [53,76]. This will need to be studied in future research, since its role in eye mechanics has not been well established.

In summary, from this work it could be predicted that the most important biomechanical risk factors for glaucoma development would be in their order of influence: a high IOP, a low CSFP and a high SAS stiffness. This would increase the A-P displacements and deformations in the ONH and PPR, and especially the strains in the A-P direction, which would cause important compressive effect to occur. The influence of these factors on the ONH would be principally focused on the central region of the LC and prelaminar tissue, where the highest A-P strains and displacements would happen. Likewise, the effect of these factors on the PPR would be primarily centred in the retina and, to a much lesser extent, in the choroid.

We would like to highlight the importance of reconstructing the eye anatomy as completely as possible. In this study, the implications of eye biomechanics have mainly been considered for glaucoma. Notwithstanding, they could also be of importance for other diseases, such as ocular hypotony, intracranial hypertension and hypotension, among others.

5. Main conclusions

The normal anatomical configuration of the human eye appears to protect the nervous tissue of the peripapillary retina, prelaminar and postlaminar tissue by allowing them to support a small amount of distortion energy.

During IOP fluctuations, the highest ONH strain values are located in the prelaminar tissue and not primarily in the LC. Despite this, LC experiences a greater A-P compression, as well as greater S-I and T-N extension, than the prelaminar tissue, with the major affectation

Table 2
Models results compared with data from experimental and clinical studies. A-P-D (anterior-posterior displacement), A-P-S (anterior-posterior strain).

Reported parameter	Reference	Specie	Reported ΔIOP (mmHg)	Time (minutes)	Reported Δ unit	Abs Δ unit/Δ mmHg Experimental	Abs Δ unit/Δ mmHg Model 1	Abs Δ unit/Δ mmHg Model 2	Qualitative accuracy Model 1	Qualitative accuracy Model 2	Relative error Model 1	Relative error Model 2
PRE A-P-D (μm) (young)	22	Human	12.2	2	−19.600	1.607	0.157	0.130	Yes	Yes	−90.215	−91.920
PRE A-P-D (μm)	16	Human	12.4	1	−42.036	3.390	0.157	0.130	Yes	Yes	−95.363	−96.171
PRE A-P-S (%)	23	Monkey	35	60	−12.000	0.343	0,032	0.033	Yes	Yes	−90.764	−90.353
PPR A-P-S (%)	21	Non-human primate	35	60	−4.800	0.137	0.102	0.106	Yes	Yes	−25.280	−22.399
PPR A-P-S (%)	20	Rodent	35	10	−8.000	0.229	0.102	0.106	Yes	Yes	−55.168	−53.439
PPR A-P-S (%)	20	Rodent	35	30	−9.000	0.257	0.102	0.106	Yes	Yes	−60.149	−58.613
PPR A-P-S (%)	20	Rodent	35	60	−11.000	0.314	0.102	0.106	Yes	Yes	−67.395	−66.138
PPR A-P-S (%)	20	Rodent	55	10	−5.700	0.104	0.102	0.106	Yes	Yes	−1.122	2.690
PPR A-P-S (%)	20	Rodent	55	30	−6.300	0.115	0.102	0.106	Yes	Yes	−10.539	−7.090
PPR A-P-S (%)	20	Rodent	55	60	−6.000	0.109	0.102	0.106	Yes	Yes	−6.066	−2.444
PPR A-P-S (%)	21	Non-human primate	35	60	−1.100	0.031	0.102	0.106	Yes	Yes	226.051	238.622
PPC A-P-S (%)	10	Human	26.1	Acute attacks	−0.118	0.005	0.020	0.021	Yes	Yes	340.101	357.611
PPC A-P-S (%)	11	Human	10.1	5	−4.740	0.469	0.020	0.021	Yes	Yes	−95.771	−95.603
PPC A-P-S (%)	20	Rodent	35	10	−9.400	0,269	0.020	0.021	Yes	Yes	−92.610	−92.316
PPC A-P-S (%)	20	Rodent	35	30	−12.700	0.363	0.020	0.021	Yes	Yes	−94.530	−94.312
PPC A-P-S (%)	20	Rodent	35	60	−8.100	0.231	0.020	0.021	Yes	Yes	−91.424	−91.083
PPC A-P-S (%)	20	Rodent	55	10	−15.000	0.273	0.020	0.021	Yes	Yes	−92.722	−92.433
LC A-P-D (μm) (european)	16	Human	11.5	1	9.750	−3.340	−0.006	−0.025	Yes	Yes	−99.812	−99.251
LC A-P-D (μm) (african)	16	Human	15	1	−19.000	3.920	−0.006	−0.025	No	No	−100.160	−100.638
LC A-P-D (μm) (young)	22	Human	12.2	2	−2.000	0.164	0.019	−0.025	Yes	No	−88.205	−115.255

Table 3
Model results compared with data from experimental and clinical studies. TPS (third principal strain), FPS (first principal strain).

Reported parameter	Reference	Specie	Reported Δ CSFP (mmHg)	Time (minutes)	Reported Δ unit	Abs Δ unit/Δ mmHg Experimental	Abs Δ unit/Δ mmHg Model 2	Qualitative accuracy	Relative error Model 2
LC TPS (%)	70	Porcine	26	60	−3.500	0.135	−0.035	No	−126.190
LC FPS (%)	70	Porcine	26	60	4.400	0.169	−0.025	No	−115.012
A-POST TPS (%)	70	Porcine	26	60	−9.100	0.350	0.021	Yes	−94.091
A-POST FPS (%)	70	Porcine	26	60	9.500	0.365	0.044	Yes	−87.860

located in the central zone of both structures.

Although all PPR layers show thinning when an increase in IOP occurs, the retina is affected the most.

IOP fluctuations cause more strains in the PPR, LC and prelaminar tissue than CSFP variations, corroborating the major role of IOP in glaucoma genesis. Nevertheless, the postlaminar tissue is more affected by CSFP changes than IOP variations.

Elevated IOP associated with low CSFP produces an increment in the strains of the peripapillary retina, peripapillary choroid, as well as in the LC central and medial region. Furthermore, it produces a change in postlaminar tissue mechanics, and posterior displacement of central and medial regions of the prelaminar tissue and LC. This probably increases the susceptibility to develop glaucoma.

Low IOP and high CSFP cause a synergistic mechanical effect on postlaminar tissue, with an incremented S-I and T-N compression and an increase in A-P extension; consequently, it can be predicted that ocular hypotension would facilitate the establishment of papilledema.

In the same way, high IOP and low CSFP cause a synergistic mechanical effect on postlaminar tissue, which is inverse to that observed with a low IOP and a high CSFP, with an incremented S-I and T-N extension and an increase in A-P compression.

SAS stiffness could increase the susceptibility to develop glaucoma, since it has a strong influence on ONH and PPR strains. However, the clinical impact of this also depends on the distribution of this variable within the population, which is unknown to date.

The meninges alter the ONH biomechanical response to IOP variations, producing a reduction in ONH strains due to ocular pressure fluctuations, which is especially significant for the postlaminar tissue. The dura mater, for its part, reduces the retinal and choroidal strains due to CSFP variations.

The most important mechanical factors for glaucoma development seem to be in their order of impact: a high IOP, a low CSFP, and high stiffness of the SAS. This would mainly affect the central region of the LC and prelaminar tissue in the ONH, as well as the retina in the PPR.

6. Limitations

This work has some limitations, since most tissues have been considered homogeneous, elastic, linear and isotropic, which does not reflect their real mechanical behaviour, although it does represent an initial approximation. In addition, due to the lack of information for human tissues, particularly for the optic nerve, some non-human properties and data from other anatomical localizations had to be used. Since tissues may exhibit different mechanical properties among species and different anatomical sites, this could lead to a major factor of error. It must be clarified that in this paper, when possible, human data was employed.

Moreover, a general two-dimensional anatomical model was constructed, and even though it was partially adapted to specific measures, it does not reflect the exact and complex three-dimensional eye anatomy, which involves important regional changes in thickness and in mechanical properties. It also does not reflect the presence of additional anatomical structures, such as the vascular bed and the extraocular muscles, all of which could be of great importance. In this research, an idealized spherical form was assumed; however, myopia, which occurs with an altered ocular anatomy and shape [77,78], is a proven risk factor for the development of glaucoma [79,80]. Therefore, studying the impact of the eye shape and geometric variations on the biomechanics of the posterior region of the eye would be of significant importance.

In addition, we have used data from just one subject, which is a major limitation, and the geometric model is not completely patient-specific. Since the structure of the optic head is different among individuals, in the future it would be necessary to develop a patient-specific orbit model on which the conclusions presented here could be validated. Additionally, the anatomy and material properties of normal and early-glaucoma eyes could differ significantly. Therefore, it would be important to develop a model with these specific characteristics, which would provide valuable information for the understanding of this disease; to date, available data are still limited.

Furthermore, the effects of the body position and head posture in the IOP have not been considered. Since different studies in diverse clinical populations have proven a significant increase in IOP when going from supine decubitus to lateral [81,82], and an IOP elevation in a low head position compared with neutral head [83,84], it would be important to consider these factors in future works. Lastly, the SAS damping function and CSFP have been modelled separately. In future studies, it will be necessary to integrate these two biomechanical characteristics in a single multiphysical model.

Data availability

The data used to support the findings of this study are available from the corresponding author upon request.

Conflicts of interest

The authors declare that there is no conflict of interests regarding the publication of this paper.

Etical statement

The authors declare that this work has followed all the ethical principles.

Funding

This research did not receive any specific grant from funding agencies in the public, commercial, or not-for-profit sectors.

Acknowledgments

All thanks are due to Doctor Eduardo Arenas, professor of ophthalmology, for his collaboration and support.

Appendix A. Supplementary data

Supplementary data to this article can be found online at https://doi.org/10.1016/j.imu.2019.100185.

References

[1] Tham YC, Li X, Wong TY, Quigley HA, Aung T, Cheng CY. Global prevalence of glaucoma and projections of glaucoma burden through 2040: a systematic review and meta-analysis. Ophthalmology 2014;121:2081–90. https://doi.org/10.1016/j.ophtha.2014.05.013.

[2] Agarwal Renu, Gupta Suresh K, Agarwal Puneet, Saxena Rohit, Agrawal Shyam S. Current concepts in the pathophysiology of glaucoma. Indian J Ophthalmol 2009;57:257–66. https://doi.org/10.4103/0301-4738.53049.

[3] Weinreb Robert N, Aung Tin, Felipe A, Medeiros. The pathophysiology and treatment of glaucoma: a review. J Am Med Assoc 2014;311:1901–11. https://doi.org/10.1001/jama.2014.3192.

[4] Kersey T, Clement CI, Bloom P, Cordeiro MF. New trends in glaucoma risk, diagnosis & management. Indian J Med Res 2013;137:659–68.

[5] Kampougeris G, Spyropoulos D, Mitropoulou A, Zografou A, Kosmides P. Peripapillary retinal nerve fiber layer thickness measurement with SD-OCT in normal and glaucomatous eyes: distribution and correlation with age. Int J Ophthalmol 2013;6:662–5. https://doi.org/10.3980/j.issn.2222-3959.2013.05.21.

[6] Chang RT, Singh K. Glaucoma suspect: diagnosis and management. Asia Pac J Ophthalmol (Phila). 2016;5:32–7. https://doi.org/10.1097/APO.0000000000000173.

[7] Zhang C, Tatham AJ, Medeiros FA, Zangwill LM, Yang Z, Weinreb RN. Assessment of choroidal thickness in healthy and glaucomatous eyes using swept source optical coherence tomography. PLoS One 2014;9:e109683https://doi.org/10.1371/journal.pone.0109683.

[8] Park HY, Lee NY, Shin HY, Park CK. Analysis of macular and peripapillary choroidal thickness in glaucoma patients by enhanced depth imaging optical coherence tomography. J Glaucoma 2014;23:225–31. https://doi.org/10.1097/IJG.0000000000000045.

[9] Banitt M. The choroid in glaucoma. Curr Opin Ophthalmol 2013;24:125–9. https://doi.org/10.1097/ICU.0b013e32835d9245.

[10] Song W, Huang P, Dong X, Li X, Zhang C. Choroidal thickness decreased in acute primary angle closure attacks with elevated intraocular pressure. Curr Eye Res 2016;41:526–31. https://doi.org/10.3109/02713683.2015.1037002.

[11] Wang YX, Jiang R, Ren XL, Chen JD, Shi HL, Xu L, Wei WB, Jonas JB. Intraocular pressure elevation and choroidal thinning. Br J Ophthalmol 2016;100:1676–81. https://doi.org/10.1136/bjophthalmol-2015-308062.

[12] Downs JC, Ensor ME, Bellezza AJ, Thompson HW, Hart RT, Burgoyne CF. Posterior scleral thickness in perfusion-fixed normal and early-glaucoma monkey eyes. Investig Ophthalmol Vis Sci 2001;42:3202–8.

[13] Ren R, Wang N, Li B, Li L, Gao F, Xu X, Jonas JB. Lamina cribrosa and peripapillary sclera histomorphometry in normal and advanced glaucomatous Chinese eyes with various axial length. Investig Ophthalmol Vis Sci 2009;50:2175–84. https://doi.org/10.1167/iovs.07-1429.

[14] Jonas SB, Jonas JB. Peripapillary sclera thickness in human eyes with glaucoma. Acta Ophthalmol 2011;89:e659–61. https://doi.org/10.1111/j.1755-3768.2010.02034.x.

[15] Yang H, Downs JC, Girkin C, Sakata L, Bellezza A, Thompson H, Burgoyne CF. 3-D histomorphometry of the normal and early glaucomatous monkey optic nerve head: lamina cribrosa and peripapillary scleral position and thickness. Investig Ophthalmol Vis Sci 2007;48:4597–607.

[16] Fazio MA, Johnstone JK, Smith B, Wang L, Girkin CA. Displacement of the lamina cribrosa in response to acute intraocular pressure elevation in normal individuals of african and european descent. Investig Ophthalmol Vis Sci. 2016 2016;57:3331–9. https://doi.org/10.1167/iovs.15-17940.

[17] Lee EJ, Kim TW, Weinreb RN, Kim H. Reversal of lamina cribrosa displacement after intraocular pressure reduction in open-angle glaucoma. Ophthalmology 2013;120:553–9. https://doi.org/10.1016/j.ophtha.2012.08.047.

[18] Lee EJ, Kim TW. Lamina cribrosa reversal after trabeculectomy and the rate of progressive retinal nerve fiber layer thinning. Ophthalmology 2015;122:2234–42. https://doi.org/10.1016/j.ophtha.2015.07.020. Epub 2015 Aug 19.

[19] Barrancos C, Rebolleda G, Oblanca N, Cabarga C, Muñoz-Negrete FJ. Changes in lamina cribrosa and prelaminar tissue after deep sclerectomy. Eye 2014;28:58–65. https://doi.org/10.1038/eye.2013.238. Epub 2013 Nov 15.

[20] Fortune B, Choe TE, Reynaud J, Hardin C, Cull GA, Burgoyne CF, Wang L. Deformation of the rodent optic nerve head and peripapillary structures during acute intraocular pressure elevation. Investig Ophthalmol Vis Sci 2011;52:6651–61. https://doi.org/10.1167/iovs.11-7578.

[21] Fortune B, Yang H, Strouthidis NG, Cull GA, Grimm JL, Downs JC, Burgoyne CF. The effect of acute intraocular pressure elevation on peripapillary retinal thickness, retinal nerve fiber layer thickness, and retardance. Investig Ophthalmol Vis Sci 2009;50:4719–26. https://doi.org/10.1167/iovs.08-3289.

[22] Agoumi Y, Sharpe GP, Hutchison DM, Nicolela MT, Artes PH, Chauhan BC. Laminar and prelaminar tissue displacement during intraocular pressure elevation in glaucoma patients and healthy controls. Ophthalmology 2011;118:52–9. https://doi.org/10.1016/j.ophtha.2010.05.016.

[23] Strouthidis NG, Fortune B, Yang H, Sigal IA, Burgoyne CF. Effect of acute intraocular pressure elevation on the monkey optic nerve head as detected by spectral domain optical coherence tomography. Investig Ophthalmol Vis Sci 2011;52:9431–7. https://doi.org/10.1167/iovs.11-7922.

[24] Reis AS, O'Leary N, Stanfield MJ, Shuba LM, Nicolela MT, Chauhan BC. Laminar displacement and prelaminar tissue thickness change after glaucoma surgery imaged with optical coherence tomography. Investig Ophthalmol Vis Sci 2012;53:5819–26. https://doi.org/10.1167/iovs.12-9924.

[25] Azuara-Blanco A, Harris A, Cantor L, Abreu M, Weinland M. Effects of short term increase of intraocular pressure on optic disc cupping. Br J Ophthalmol 1998;82:880–3.

[26] Fatehee N, Yu PK, Morgan WH, Cringle SJ, Yu DY. The impact of acutely elevated intraocular pressure on the porcine optic nerve head. Investig Ophthalmol Vis Sci 2011;52:6192–8. https://doi.org/10.1167/iovs.10-7137.

[27] Shetty P, Hegde AM, Rai K. Finite element method–an effective research tool for dentistry. J Clin Pediatr Dent 2010;34:281–5.

[28] Feola AJ, Myers JG, Raykin J, Mulugeta L, Nelson ES, Samuels BC, Ethier CR. Finite element modeling of factors influencing optic nerve head deformation due to intracranial pressure. Investig Ophthalmol Vis Sci 2016;57:1901–11. https://doi.org/10.1167/iovs.15-17573.

[29] Sigal IA, Flanagan JG, Tertinegg I, Ethier CR. Finite element modeling of optic nerve head biomechanics. Investig Ophthalmol Vis Sci 2004;45:4378–87.

[30] Sigal IA, Flanagan JG, Ethier CR. Factors influencing optic nerve head biomechanics. Investig Ophthalmol Vis Sci 2005;46:4189–99.

[31] Wang X, Rumpel H, Lim WE, Baskaran M, Perera SA, Nongpiur ME, Aung T, Milea D, Girard MJ. Finite element analysis predicts large optic nerve head strains during horizontal eye movements. Investig Ophthalmol Vis Sci 2016;57:2452–62. https://doi.org/10.1167/iovs.15-18986.

[32] Ayyalasomayajula A, Park RI, Simon BR, Vande Geest JP. A porohyperelastic finite element model of the eye: the influence of stiffness and permeability on intraocular pressure and optic nerve head biomechanics. Comput Methods Biomech Biomed Eng 2016;19:591–602. https://doi.org/10.1080/10255842.2015.1052417.

[33] Hua Y, Tong J, Ghate D, Kedar S, Gu L. Intracranial pressure influences the behavior of the optic nerve head. J Biomech Eng 2017;139. https://doi.org/10.1115/1.4035406.

[34] Wang X, Fisher LK, Milea D, Jonas JB, Girard MJ. Predictions of optic nerve traction forces and peripapillary tissue stresses following horizontal eye movements. Investig Ophthalmol Vis Sci 2017;58:2044–53. https://doi.org/10.1167/iovs.16-21319.

[35] Feola AJ, Nelson ES, Myers J, Ethier CR, Samuels BC. The impact of choroidal swelling on optic nerve head deformation. Investig Ophthalmol Vis Sci 2018;59:4172–81. https://doi.org/10.1167/iovs.18-24463.

[36] Hou R, Zhang Z, Yang D, Wang H, Chen W, Li Z, Sang J, Liu S, Cao Y, Xie X, Ren R, Zhang Y, Sabel BA, Wang N. Intracranial pressure (ICP) and optic nerve subarachnoid space pressure (ONSP) correlation in the optic nerve chamber: the Beijing Intracranial and Intraocular Pressure (iCOP) study. Brain Res 2016;1635:201–8. https://doi.org/10.1016/j.brainres.2016.01.011.

[37] Morgan WH, Yu DY, Alder VA, et al. The correlation between cerebrospinal fluid pressure and retrolaminar tissue pressure. Investig Ophthalmol Vis Sci 1998;39:1419–28.

[38] Fleischman D, Allingham RR. The role of cerebrospinal fluid pressure in glaucoma and other ophthalmic diseases: a review. Saudi J Ophthalmol 2013;27:97–106. https://doi.org/10.1016/j.sjopt.2013.03.002. Epub 2013 Mar 17.

[39] Mayanagi K, Nakatsukasa M, Inamasu J. Cerebrospinal fluid leakage at the lumbar spine: a unique cause of delayed neurologic deterioration in a traumatic acute subdural hematoma patient. Asian J Neurosurg 2019;14:219–22. https://doi.org/10.4103/ajns.AJNS_185_17.

[40] Rangel-Castilla L, Gopinath S, Robertson CS. Management of intracranial hypertension. neurol Clin 2008;26:521–41. https://doi.org/10.1016/j.ncl.2008.02.003. x.

[41] Oyama Tokuhide, Abe Haruki, Ushiki Tatsuo. The connective tissue and glial framework in the optic nerve head of the normal human eye: light and scanning electron microscopic studies. Arch Histol Cytol 2006;69:341–56.

[42] Vurgese S, Panda-Jonas S, Jonas JB. Scleral thickness in human eyes. PLoS One 2012;7:e29692https://doi.org/10.1371/journal.pone.0029692.

[43] Xu J, Ishikawa H, Wollstein G, Bilonick RA, Kagemann L, Craig JE, Mackey DA, Hewitt AW, Schuman JS. Automated volumetric evaluation of stereoscopic disc photography. Optic Express 2010;18:11347–59. https://doi.org/10.1364/OE.18.011347.

[44] Ross M, Wojciech P. Histology: a text and Atlas, with correlated cell and molecular biology. sixth ed. Baltimore: Lippincott Williams & Wilkins; 2011. p. 381–5.

[45] Hayreh SS. Ischemic optic neuropathies. first ed. Berlin: Springer-Verlag; 2011. p. 7–34.

[46] Jonas JB, Holbach L, Panda-Jonas S. Peripapillary ring: histology and correlations. Acta Ophthalmol 2014;92:e273–9. https://doi.org/10.1111/aos.12324.

[47] Jonas JB, Holbach L. Central corneal thickness and thickness of the lamina cribrosa in human eyes. Investig Ophthalmol Vis Sci 2005;46:1275–9.

[48] Tsutsumi T, Tomidokoro A, Araie M, Iwase A, Sakai H, Sawaguchi S. Planimetrically determined vertical cup/disc and rim width/disc diameter ratios and related factors. Investig Ophthalmol Vis Sci 2012;53:1332–40. https://doi.org/10.1167/iovs.11-8533.

[49] Tariq YM, Li H, Burlutsky G, Mitchell P. Retinal nerve fiber layer and optic disc measurements by spectral domain OCT: normative values and associations in young adults. Eye 2012;26:1563–70. https://doi.org/10.1038/eye.2012.216.

[50] Knight OJ, Girkin CA, Budenz DL, Durbin MK, Feuer WJ. Cirrus OCT Normative Database Study Group. Effect of race, age, and axial length on optic nerve head parameters and retinal nerve fiber layer thickness measured by Cirrus HD-OCT. Arch Ophthalmol 2012;130:312–8. https://doi.org/10.1001/archopthalmol.2011.1576.

[51] Chen K, Weiland JD. Mechanical properties of orbital fat and its encapsulating connective tissue. J Biomech Eng 2011;133:064505https://doi.org/10.1115/1.4004289.

[52] Chen K, Rowley AP, Weiland JD, Humayun MS. Elastic properties of human posterior eye. J Biomed Mater Res A 2014;102:2001–7. https://doi.org/10.1002/jbm.a.34858.

[53] Saboori P, Sadegh A. Material modeling of the head's subarachnoid space. Sci Iran 2011;18:1492–9. https://doi.org/10.1016/j.scient.2011.11.032.
[54] Downs JC, Suh JK, Thomas KA, Bellezza AJ, Burgoyne CF, Hart RT. Viscoelastic characterization of peripapillary sclera: material properties by quadrant in rabbit and monkey eyes. J Biomech Eng 2003;125:124–31.
[55] Downs JC, Suh JK, Thomas KA, Bellezza AJ, Hart RT, Burgoyne CF. Viscoelastic material properties of the peripapillary sclera in normal and early-glaucoma monkey eyes. Investig Ophthalmol Vis Sci 2005;46:540–6.
[56] Saboori P, Sadegh A. Histology and morphology of the brain subarachnoid trabeculae. Anat Res Int 2015;2015:1–9. https://doi.org/10.1155/2015/279814.
[57] Killer HE, Laeng HR, Flammer J, Groscurth P. Architecture of arachnoid trabeculae, pillars, and septa in the subarachnoid space of the human optic nerve: anatomy and clinical considerations. Br J Ophthalmol 2003;87:777–81.
[58] Cirovic S, Bhola RM, Hose DR, Howard IC, Lawford PV, Marr JE, Parsons MA. Computer modelling study of the mechanism of optic nerve injury in blunt trauma. Br J Ophthalmol 2006;90:778–83.
[59] Kakizaki H, Takahashi Y, Nakano T, Asamoto K, Ikeda H, Ichinose A, Iwaki M, Selva D, Leibovitch I. Anatomy of tenons capsule. Clin Exp Ophthalmol 2012;40:611–6. https://doi.org/10.1111/j.1442-9071.2011.02745.x.
[60] Roy Chowdhury U, P Fautsch M. Intracranial pressure and its relationship to glaucoma: current understanding and future directions. Med Hypothesis, Discov Innovation (MEHDI) Ophthalmol 2015;4:71–80.
[61] Jonas JB, Wang N, Yang D. Translamina cribrosa pressure difference as potential element in the pathogenesis of glaucomatous optic neuropathy. Asia Pac J Ophthalmol (Phila). 2016;5:5–10. https://doi.org/10.1097/APO.0000000000000170.
[62] Voorhees AP, Jan NJ, Sigal IA. Effects of collagen microstructure and material properties on the deformation of the neural tissues of the lamina cribrosa. Acta Biomater 2017;58:278–90. https://doi.org/10.1016/j.actbio.2017.05.042.
[63] Midgett DE, Pease ME, Jefferys JL, Patel M, Franck C, Quigley HA, Nguyen TD. The pressure-induced deformation response of the human lamina cribrosa: analysis of regional variations. Acta Biomater 2017;53:123–39. https://doi.org/10.1016/j.actbio.2016.12.054.
[64] Quigley HA, Addicks EM, Green WR, Maumenee AE. Optic nerve damage in human glaucoma. II. The site of injury and susceptibility to damage. Arch Ophthalmol 1981;99:635–49.
[65] Quigley HA, Addicks EM. Chronic experimental glaucoma in primates. II. Effect of extended intraocular pressure elevation on optic nerve head and axonal transport. Investig Ophthalmol Vis Sci 1980;19:137–52.
[66] Quigley H, Anderson DR. The dynamics and location of axonal transport blockade by acute intraocular pressure elevation in primate optic nerve. Investig Ophthalmol 1976;15:606–16.
[67] Wollensak G, Spoerl E. Biomechanical characteristics of retina. Retina 2004;24:967–70.
[68] Guo L, Normando EM, Nizari S, Lara D, Cordeiro MF. Tracking longitudinal retinal changes in experimental ocular hypertension using the cSLO and spectral domain-OCT. Investig Ophthalmol Vis Sci 2010;51:6504–13. https://doi.org/10.1167/iovs.10-5551.
[69] Lei Y, Garrahan N, Hermann B, Becker DL, Hernandez MR, Boulton ME, Morgan JE. Quantification of retinal transneuronal degeneration in human glaucoma: a novel multiphoton-DAPI approach. Investig Ophthalmol Vis Sci 2008;49:1940–5. https://doi.org/10.1167/iovs.07-0735.
[70] Feola AJ, Coudrillier B, Mulvihill J, Geraldes DM, Vo NT, Albon J, Abel RL, Samuels BC, Ethier CR. Deformation of the lamina cribrosa and optic nerve due to changes in cerebrospinal fluid pressure. Investig Ophthalmol Vis Sci 2017;58:2070–8. https://doi.org/10.1167/iovs.16-21393.
[71] Faingold D, Francis CJ, Buys YM. Hypotony maculopathy and papilledema after trabeculectomy in a patient with pseudotumor cerebri. J Glaucoma 2003;12:374–8.
[72] Greenfield DS, Wanichwecharungruang B, Liebmann JM, Ritch R. Pseudotumor cerebri appearing with unilateral papilledema after trabeculectomy. Arch Ophthalmol 1997;115:423–6.
[73] Yang D, Fu J, Hou R, Liu K, Jonas JB, Wang H, Chen W, Li Z, Sang J, Zhang Z, Liu S, Cao Y, Xie X, Ren R, Lu Q, Weinreb RN, Wang N. Optic neuropathy induced by experimentally reduced cerebrospinal fluid pressure in monkeys. Investig Ophthalmol Vis Sci 2014;55:3067–73. https://doi.org/10.1167/iovs.13-13657.
[74] García-Montesinos J, Muñoz-Negrete FJ, de Juan V, Rebolleda G. Relationship between lamina cribrosa displacement and trans-laminar pressure difference in papilledema. Graefes Arch Clin Exp Ophthalmol 2017;255:1237–43. https://doi.org/10.1007/s00417-017-3661-6.
[75] Lee DS, Lee EJ, Kim TW, Park YH, Kim J, Lee JW, Kim S. Influence of translaminar pressure dynamics on the position of the anterior lamina cribrosa surface. Investig Ophthalmol Vis Sci 2015;56:2833–41. https://doi.org/10.1167/iovs.14-15869.
[76] Matsumae M, Sato O, Hirayama A, Hayashi N, Takizawa K, Atsumi H, Sorimachi T. Research into the physiology of cerebrospinal fluid reaches a new horizon: intimate exchange between cerebrospinal fluid and interstitial fluid may contribute to maintenance of homeostasis in the central nervous system. Neurol Med -Chir 2016;56:416–41. https://doi.org/10.2176/nmc.ra.2016-0020.
[77] Xu L, Li Y, Wang S, Wang Y, Wang Y, Jonas JB. Characteristics of highly myopic eyes: the beijing eye study. Ophthalmology 2007;114:121–6. Epub 2006 Oct 27.
[78] Miyake M, Yamashiro K, Akagi-Kurashige Y, Oishi A, Tsujikawa A, Hangai M, Yoshimura N. Analysis of fundus shape in highly myopic eyes by using curvature maps constructed from optical coherence tomography. PLoS One 2014;9:e107923https://doi.org/10.1371/journal.pone.0107923. eCollection 2014.
[79] Hsu CH, Chen RI, Lin SC. Myopia and glaucoma: sorting out the difference. Curr Opin Ophthalmol 2015;26:90–5. https://doi.org/10.1097/ICU.0000000000000124.
[80] Xu L, Wang Y, Wang S, Wang Y, Jonas JB. High myopia and glaucoma susceptibility the beijing eye study. Ophthalmology 2007;114:216–20. Epub 2006 Nov 21.
[81] Lee JY, Yoo C, Jung JH, Hwang YH, Kim YY. The effect of lateral decubitus position on intraocular pressure in healthy young subjects. Acta Ophthalmol 2012;90:e68–72. https://doi.org/10.1111/j.1755-3768.2011.02208.x. Epub 2011 Jul 29.
[82] Lee JY, Yoo C, Kim YY. The effect of lateral decubitus position on intraocular pressure in patients with untreated open-angle glaucoma. e2 Am J Ophthalmol 2013;155:329–35. https://doi.org/10.1016/j.ajo.2012.08.003. Epub 2012 Oct 27.
[83] Seo H, Yoo C, Lee TE, Lin S, Kim YY. Head position and intraocular pressure in the lateral decubitus position. Optom Vis Sci 2015;92:95–101. https://doi.org/10.1097/OPX.0000000000000432.
[84] Lee TE, Yoo C, Lin SC, Kim YY. Effect of different head positions in lateral decubitus posture on intraocular pressure in treated patients with open-angle glaucoma. Am J Ophthalmol 2015;160:929–36. https://doi.org/10.1016/j.ajo.2015.07.030. e4, Epub 2015 Jul 23.